TECHNICAL REPORT

CIRCULATION AND OCEANOGRAPHIC PROPERTIES IN THE SOMALI BASIN AS OBSERVED DURING THE 1979 SOUTHWEST MONSOON

WILLIAM H. BEATTY III
JOHN G. BRUCE *
ROBERT C. GUTHRIE

JUNE 1981

Approved for public release; distribution unlimited.

* Currently affiliated with Woods Hole Oceanographic Institution, Woods Hole, Mass. 02543

PREPARED BY
COMMANDING OFFICER,
NAVAL OCEANOGRAPHIC OFFICE
NSTL STATION, BAY ST. LOUIS, MS 39522

PREPARED FOR
COMMANDER
NAVAL OCEANOGRAPHY COMMAND
NSTL STATION, BAY ST. LOUIS, MS 39529

FOREWORD

The Northwest Indian Ocean, being subjected to the seasonally shifting monsoon winds, is unlike any other ocean area in the world. The strong, yet shallow, current system that is called the Somali Current or East African Current is associated with summer southwesterly monsoon winds that parallel the Somali Coast and curve eastward in the vicinity of Cape Guardafui. The Somali Current is rapid (≈350 cm sec^{-1} in some places) yet shallow (<500 m). Volume transports associated with the Somali Current south of Socotra Island have been found to be between 60 and 70 sverdrups, roughly comparable to those found in the Gulf Stream. Unlike the Gulf Stream, the Somali Current has been known to disappear and even reverse during the winter months of the northeast monsoon.

The strategic importance of this region places a special burden on the naval environmentalist to gain an adequate understanding of the oceanography and meteorology of the Somali Basin/Arabian Sea area. Although the Somali Basin is quite deep (>5000 m in parts of the abyssal plain), most of the area is bottom-limited for convergence zone propagation. Shallow sound channels caused by interleaving of Red Sea and Persian Gulf Waters may have tactical implications in the employment of acoustic weapons and sensors. High seas with sustained w d in the region of Cape Guardafui a of the southwest monsoon.

This Techn reader a general idea of general bbserved during the 1979 southwest eak and late and was characterized b

SECURITY CLASSIFICATION OF THIS PAGE *(When Data Entered)*

REPORT DOCUMENTATION PAGE

READ INSTRUCTIONS BEFORE COMPLETING FORM

1. REPORT NUMBER: TR-258
2. GOVT ACCESSION NO.:
3. RECIPIENT'S CATALOG NUMBER:

4. TITLE *(and Subtitle)*: Circulation and Oceanographic Properties in the Somali Basin as Observed During the 1979 Southwest Monsoon

5. TYPE OF REPORT & PERIOD COVERED: Technical Report

6. PERFORMING ORG. REPORT NUMBER:

7. AUTHOR(s): Beatty, William H. III; Bruce, John G.; Guthrie, Robert C.

8. CONTRACT OR GRANT NUMBER(s):

9. PERFORMING ORGANIZATION NAME AND ADDRESS: Naval Oceanographic Office, NSTL Station, Bay St. Louis, Mississippi 39522

10. PROGRAM ELEMENT, PROJECT, TASK AREA & WORK UNIT NUMBERS:

11. CONTROLLING OFFICE NAME AND ADDRESS:

12. REPORT DATE: June 1981

13. NUMBER OF PAGES:

14. MONITORING AGENCY NAME & ADDRESS *(if different from Controlling Office)*:

15. SECURITY CLASS. *(of this report)*: Unclassified

15a. DECLASSIFICATION/DOWNGRADING SCHEDULE:

16. DISTRIBUTION STATEMENT *(of this Report)*

Approved for public release; distribution unlimited.

17. DISTRIBUTION STATEMENT *(of the abstract entered in Block 20, if different from Report)*

18. SUPPLEMENTARY NOTES

John G. Bruce is currently affiliated with Woods Hole Oceanographic Institution

19. KEY WORDS *(Continue on reverse side if necessary and identify by block number)*

Indian Ocean, Southwest Monsoon, Somali Current, Somali Front, East African Current, Fronts, Eddies, Currents, Physical Oceanography, Indian Ocean Surveys, Oceanographic Stations, XBTs.

20. ABSTRACT *(Continue on reverse side if necessary and identify by block number)*

Shipboard expendable bathythermograph (XBT), salinity-temperature-depth (STD), and sea surface temperature and salinity observations were taken from USNS WILKES (T-AGS 33) from 16 August until 5 September 1979 in the area of the Somali Current off the coast of Northeast Africa. Analysis of the data indicated the presence of two large anti-cyclonic gyres. The larger of the two gyres, called the Great Whirl or Prime Eddy, was centered at about 7°N and 55°E with a diameter of approximately 350 nautical miles. The smaller

DD FORM 1 JAN 73 1473 EDITION OF 1 NOV 65 IS OBSOLETE S/N 0102-014-6601

SECURITY CLASSIFICATION OF THIS PAGE *(When Data Entered)*

gyre, known as the Socotra Eddy, was centered at approximately 12°N and 57°E with an approximate diameter of 200 nautical miles. The two eddies were separated by a trough of cold water advected from the region of upwelling off the Somali coast between 9°N and 11°N. Studies of TIROS-N satellite infrared photographs and XBT cross-sections taken from tankers transiting the area during July and early August 1979 indicated the presence of a southern eddy separated from the Great Whirl by a trough of cold, upwelled water between 3°N and 5°N. During the early part of the WILKES survey, the southern eddy and the Great Whirl coalesced.

ACKNOWLEDGMENTS

We are indebted to the master, officers, and crew of USNS WILKES for their help and cooperation in obtaining scientifically significant data. Mr. Charles Horton and Mr. Alvan Fisher, Jr., critically reviewed the manuscript, and Mr. Ray Floyd and Ms. Rose Gorski helped with the plotting and analysis of the data. Mr. Glen Voorheis did the illustrations, and Ms. Jo Ann Lyons, Ms. Cathy Shedd, Ms. B. J. Dauro and Ms. Linda-Anne Stanley provided secretarial assistance. Mr. Leon Parke was Senior Naval Oceanographic Office (NAVOCEANO) Representative on board USNS WILKES.

Special thanks are due EXXON Corporation for use of their tankers. The Office of Naval Research provided finanacial support to the XBT tanker section program under grant N00014-79-C-0071, NR083-004 to Woods Hole Oceanographic Institution (J. G. Bruce). This grant was also for the general planning and arrangements of USNS WILKES' participation in the INDEX program during the 1979 southwest monsoon. Thanks are also due the University of Capetown whose observers obtained all tanker XBT data.

CONTENTS

FIGURES

I. INTRODUCTION - GENERAL CHARACTERISTICS OF THE AREA

An oceanographic survey of the area between the Horn of Africa and the meridian of 60°E was conducted from USNS WILKES (T-AGS 33) during August and September of 1979. This is the region of the Somali Current, Somali Front, or East African Current, which are names given to the large ocean circulation system influenced by the southwest monsoon. The southwest monsoon, caused by differential solar heating of the vast Afro-Asian land mass and the Indian Ocean on its southern and eastern boundaries, is a seasonal wind that blows along the coast of East Africa and bends to the northeast as it crosses the Horn of Africa beginning in May and ending in September. Although oceanographers and meteorologists are in general agreement concerning the existence of a causal link between the southwest monsoon and the shallow but rapid transport of water northeastward that is called the Somali Current, the exact nature of the processes involved is not clearly understood. In particular, the effects of a strong and rapidly varying wind stress on the sea surface topography in low latitudes are poorly understood (Warren et al., 1966).

One of the difficulties in understanding the dynamics of the Somali Current is posed by the necessity of separating the barotropic from the baroclinic field of mass. Hurlburt and Thompson (1976) characterize the Somali Current as a time-dependent, baroclinic, inertial boundary current. The large anticyclonic gyre south of Socotra Island, accompanied by supergeostrophic flow, is characterized by anticyclonic inflow in the upper layer and cyclonic outflow in the lower layer (Hurlburt and Thompson, 1976). Lighthill (1969) in ascribing the formation of the Somali Current to mass flux deposited by baroclinic and barotropic waves in the western boundary region neglects wind stress acting within 500 km of the coast. However, Leetma (1972; 1973) found that local winds are crucial to the onset of the Somali Current.

Although theoretical models have undoubtedly contributed a great deal to an improved understanding of the Somali Current, they are incomplete. They must be supplemented by future ship and aircraft surveys in the area owing to the relative paucity of oceanographic surveys dedicated to a thorough understanding of the Somali Current. Standard sections allowing time-series analyses, such as have been completed from EXXON tankers transiting the area, would be of great value in achieving an improved understanding of the temporal evolution of the Somali Current (Bruce, 1979). Figure 1 presents the location of the sea lane transited by the EXXON tankers during the taking of the XBT cross-sections.

Although the amount of historical data available from this area is considerable, it is of limited value in understanding the fine structure of the strong and highly variable Somali Current. Colborn (1975) performed an excellent climatological analysis of the entire Indian Ocean from a total of 28,669 bathythermograph and hydrocast observations distributed among 274 subareas. Poor distribution of the observations in both space and time, together with aliasing and averaging, makes it impractical to glean from them the fine structure of the complex Somali Current System.

Although the Somali Current is found on the western boundary of the Indian Ocean off the Horn of Africa and thus has been called a "western boundary current", it differs in several important respects from the Gulf

Stream and Kuroshio. Driven principally by the monsoon wind system characteristic of this part of the world it is the most seasonably variable of the major ocean currents. Although the Gulf Stream and Kuroshio show significant variations in the form of meanders and eddies, such variations are small compared with the mean circulation of these two mid-latitude western boundary currents. The Somali Current, on the other hand, is known from reports of ship set and drift to disappear and even reverse in surface and near-surface layers during the months of the northeast monsoon.

The Somali Current has been found to be a comparatively shallow current. Düing (1970), in a statistical study of dynamic height anomalies from all months in the Indian Ocean north of 20°S, found the dynamic height anomalies of the 1000 and 2000 dbar surfaces relative to the 3000 dbar surface to be almost randomly distributed in a Gaussian distribution indicating the absence of significant horizontal baroclinic pressure gradients at these levels. Values of 600 dbar relative to 3000 dbar were found to depart from the random distribution indicating the presence of geostrophic motion at 600 dbar relative to the 3000 dbar surface. Studies of surface dynamic height values with respect to 1000 dbar from July, August, and September only showed a very broad non-Gaussian distribution which is indicative of appreciable horizontal pressure gradients and strong geostrophic currents at the surface relative to 1000 dbar. This shallowness of circulation of the western Indian Ocean seems reasonable in light of the extreme variability of the monsoon winds in this area. In the deeper layers, below 1000 dbar, the field of mass probably does not have time to adjust to rapid changes in wind stress at the surface. In the western Atlantic and Pacific Oceans where isopycnals show an appreciable slope below 2000 m, the surface wind stress clearly shows less annual variation than in the northwestern Indian Ocean where the prevailing winds shift from northeasterly in January and February to southwesterly in July and August. In the great western boundary currents of the North Atlantic and Pacific Oceans, there is time for the field of mass to adjust to a much greater depth owing to the more persistent surface wind stress. Although there has been considerable controversy among classical oceanographers concerning the placement of a reference level or level of no motion in both the Gulf Stream and Kuroshio (Stommel, 1966), such a level occurs at a much shallower depth in the Somali Current system.

The rapid response of the Somali Current needs to be understood in terms of the modal structure of baroclinic waves. It is not sufficient to ascribe the Somali Current to a mere local response of the ocean to the local winds (Lighthill, 1969). The Somali Current is highly baroclinic and is spun up within a month of the onset of the southwesterly monsoon winds. Although the barotropic and the baroclinic spin up times are comparable at the low latitudes of the Somali Current system, the baroclinic mode is the dominant mode (Düing and Szekelda, 1971).

From his studies of the historical ocean data in the Indian Ocean, Düing (1970) surmised the presence of alternative cyclonic and anticyclonic gyres in this area. These Indian Ocean gyres, inferred from dynamic topographies calculated from a total of 4,390 oceanographic stations from the entire Indian Ocean, were found to be about 300 to 500 nmi in extent. This is considerably larger than the meanders and eddies associated with the Gulf Stream and Kuroshio which are on the order of 50 to 100 nmi in diameter. Although the

pattern of alternative gyres was found to persist throughout the year, it was found to be most prominent in July, August, and September. The two large anticyclonic gyres, the Great Whirl or Prime Eddy and the Socotra Eddy, together with the strong shear zone along the eastern edge of the Great Whirl observed from USNS WILKES during late August and early September of 1979, are evidence of this multi-cellular circulation. Circulation of this kind attests to the considerable complexity and variability of the Somali Current system.

One of the principal difficulties in obtaining a true picture of the circulation in the area was the asynopticity of the data taken from USNS WILKES. Unlike the meteorologist who relies on synoptic observations to display and analyze weather observations on a map, the oceanographer must rely on observations taken over a period of several days or weeks. Fortunately, changes in the ocean are normally slow enough to permit meaningful analyses of data taken from a single survey ship during a single cruise. However, recent studies of satellite photographs and time-series XBT sections have indicated much more rapid and pronounced oceanic variability than has been assumed in classical oceanographic surveying and analysis. The satellite imagery from 18 to 27 August 1979 (figures 2 and 3, respectively) amply illustrates the magnitude of the changes that can occur during such a short time as nine days. The ribbon of cold upwelled water between the Southern Eddy and the Great Whirl that appears in the 18 August imagery is not evident at the surface in the 27 August imagery. Such rapid changes lead to considerable difficulty in the analyses of observations that are close to each other in space, yet taken 12 days apart at nearly the same geographical location (figure 4). Observations 154 and 344 are especially effective illustrations of the analytical difficulties posed by a rapidly changing environment. Between 20 August 1979 and 1 September 1979 the 20°C isotherm rose 138 m.

II. METHODS

The survey was conducted from USNS WILKES (T-AGS 33) from 16 August until 5 September 1979. Four hundred fifteen successful shipboard expendable bathythermograph (XBT) observations were taken, together with 27 salinity-temperature-depth (STD) stations. The XBTs, Sippican Model T-4 and T-7 probes, provided temperature profiles to approximately 450 m and 750 m respectively. The STD stations, taken with the Plessey Model 9040 STD, were taken to a depth of at least 1500 m. Also, sea surface temperature was monitored continuously with a Model 2801A Hewlett Packard quartz crystal thermometer mounted on the hull two feet below the water line. Hourly sea surface temperatures were taken with a bucket thermometer, together with sea surface salinity samples every two hours. At each STD station, salinity samples were also taken with a Niskin rosette sampler to assist in field calibration of the salinometer. All salinity samples were stored at room temperature for at least 24 hours in citrate of magnesia bottles before being measured with an Autosal Model 8400 induction salinometer. The STD data were processed and field calibrations were performed in accordance with instructions by Beller, et al. (1975). Offset corrections were derived and applied in the field, and the resultant temperature and salinity values were found to be accurate within 0.02°C and 0.02 °/oo, respectively. Figure 5 presents track lines and locations of STD and XBT drops during the survey.

III. TEMPERATURE SECTIONS

Figure 6 is a temperature section (section 1) based on XBT data taken between the Seychelles plateau and the Somali Coast from 16 to 19 August 1979. Approaching the equator from the south, a gradual deepening and packing of isotherms in the upper 150 m is observed. This is indicative of a shallow (<150 m) easterly-flowing countercurrent between the Seychelles plateau and the equator. The sharp downslope of isotherms between 560 and 580 nmi is indicative of strong horizontal shear. Between 300 and 400 nmi from the coast, packing of isotherms between 20°C and 15°C straddling the equator is especially noticeable. The observation is at variance with equatorial observations in the Atlantic and Pacific, which generally reveal spreading of isotherms on sections crossing the equator. In these two oceans, southeast tradewinds crossing the equator are the cause of mass divergence along the equator, giving rise to an upward displacement of the thermocline (Neumann and Pierson, 1966). Such is not the case in the western Indian Ocean during the southwest monsoon, when the winds crossing the equator have a westerly instead of an easterly component. The deepening and packing of isotherms observed on this section in the immediate vicinity of the equator are the result of mass convergence at the equator caused by southerly monsoon winds blowing across the equator with a slight westerly component. The current shear appears to be quite weak in the region of the equator as inferred from the relatively gentle slope of the isotherms. The abrupt peaking of isotherms between 22°C and 25°C at approximately 260 nmi is an indication of strong shear in the upper 100 m. This peaking of isotherms is coincident with the strong gradient in sea surface salinity (figure 19) just north of the equator and is an indication of a zone of transition between relatively fresh water (S<35.1 °/oo) in the near-coastal circulation and the more saline oceanic water to the east. The sinking of isotherms from the coast out to 200 nmi indicates northeastward-setting geostrophic flow.

Section 2, depicted in figure 7, is a temperature cross-section based on XBT data taken from 19 to 22 August across the center of the Great Whirl. The sharp slope of isotherms near the coast is especially pronounced out to about 250 nmi. As the colder isotherms (T<20°C) level off, two major breaks in the data are encountered. These breaks are the result of repeated failures to achieve successful XBT drops below about 200 m. Between 290 and 310 nmi a weak front in the upper 100 m is evident in the sharp upturning and breaking of the surface of the 24°C and 25°C isotherms. Particularly sharp upsloping of isotherms is noticeable between 500 nmi and 580 nmi. The 20°C isotherm rises 100 m in 60 nmi between 520 and 580 nmi from the Somali coast. The sharp deepening of isotherms between 580 nmi from the coast to the end of the section is also noticeable. The 20°C isotherm deepens from 80 m at 580 nmi to about 150 m at the end of the section. Of particular interest is the pronounced reversal in slope of the isotherms between 500 nmi and 640 nmi from the coast.

Section 3, shown in figure 8, is about 90 miles long and contains nine observations. This section parallels the front which forms the eastern edge of the Great Whirl and was a traverse made to avoid crossing the Great Whirl at the same place. The thermocline rises slightly between 50 and 90 nmi indicating an easterly-setting geostrophic current. However, the major component of the current is most likely meridional since this section parallels rather than crosses the front.

Section 4, shown in figure 9, is 500 nmi long and was taken between 23 and 26 August. It is a recrossing of the Great Whirl close to its northern boundary in order to assess the area of maximum upwelling. From the end of the section until about 460 nmi from the coast the warmer isotherms ($T>15^{o}C$) slope sharply upward. The $25^{o}C$ and $24^{o}C$ isotherms break the surface between 460 and 480 nmi from the coast, and the $23^{o}C$ isotherm rises by about 70 m in less than 20 nmi. Between 460 and about 310 nmi from the coast all isotherms slope downward with the warmer ($T>20^{o}C$) isotherms showing the strongest downward slope. A weak near-surface front is evident 300 nmi from the coast. Again, this weak near-surface front is coincident with a strong sea surface salinity gradient (figure 19) marking a zone of transition between relatively fresh ($S<35.0\ ^{o}/oo$) coastal and equatorial water and more saline ($S>35.6\ ^{o}/oo$) oceanic water of Arabian Sea origin to the east. Within 300 nmi of the coast there is a general shoaling of all isotherms with the most pronounced shoaling occurring within 100 nmi of the coast. The rise of the $14^{o}C$ isotherm from 250 m at 180 nmi to 35 m at 10 nmi is an indication of the intense baroclinicity of the coastal current in the area. Close to the Somali Coast at the end of the section the sea surface temperature dropped from $22^{o}C$ to less than $15^{o}C$ in seven miles. The maximum currents were estimated from ship set and drift measurements to be in excess of 5 knots.

Sections 5 and 6, taken between 26 and 29 August and shown in figures 10 and 11, respectively, cross the complex boundaries between the relatively cold water off Ras Mabber at about $9^{o}N$, the northern boundary of the Great Whirl, and the southwestern edge of the Socotra Eddy. Along section 5 the $15^{o}C$ isotherm rises 170 m in less than 180 nmi, and the $16^{o}C$ isotherm breaks the surface just off the coast. The $20^{o}C$ isotherm breaks the surface at locations 60 and 80 nmi from the coast. This patch of cold ($T<20^{o}C$) surface water is located about 60 nmi southeast of Ras Hafun and is collocated with a strong gradient in sea surface salinity (figure 19). The cold water in this region is also evident in the NOAA TIROS-N satellite infrared imagery of 27 August (figure 3). From both satellite imagery and XBT observations it is evident that this region was undergoing rapid and complex changes at the time of the observations.

Section 6, taken between 27 and 29 August, was made to study the circulation immediately to the south of Socotra Island. The slope of isotherms is somewhat gradual for the first 200 nmi of the section. This gradual downslope is followed by a sharper upslope between 200 nmi and the end of the section. In 80 nmi the $20^{o}C$ isotherm rises over 100 m. This sharp upslope of isotherms is coincident with a very complex and irregular surface salinity field (figure 19) and is associated with the zone of transition between coastal Somali Current water and water of Arabian Sea origin.

Section 7 (figure 12) crosses the approximate center of the Socotra Eddy from 29 to 30 August. There is a general downslope of isotherms out to about 180 nmi with the $20^{o}C$ isotherm deepening by about 180 m. This deepening of isotherms is coincident with maximum sea surface salinities ($S>35.9\ ^{o}/oo$) (figure 19). Between 180 nmi and the end of the section there is a pronounced and general upslope of the isotherms. The $20^{o}C$ isotherm rises from 210 m at 180 nmi to 105 m at the end of the section. Breaks in the isotherms are indications of repeated XBT failures. The general bowl-shaped structure of the isotherms in this section indicates the presence of an anticyclonic eddy

that is separate from and considerably smaller than the Great Whirl (about 200 nmi).

Section 8 (figure 13), taken between 30 and 31 August, shows extended coverage of the eastern edge of the Socotra Eddy. The downslope of isotherms out to 100 nmi indicates a frontal zone accompanied by strong vertical shear. This front is probably the boundary between the northern edge of the Socotra Eddy and the Gulf of Aden/Arabian Sea circulation system. The gradual rise of isotherms between 100 and 200 nmi is indicative of southwesterly flow around the eastern extremity of the Socotra Eddy; Arabian Sea water may be entrained into the Socotra Eddy. The downslope of isotherms in the last 80 nmi of the section is an indication that the section has crossed the front separating the Socotra Eddy from the Arabian Sea.

Section 9 (figure 14) was made to recross the Great Whirl to assess any changes that may have occurred during the decay of the southwest monsoon and was taken between 31 August and 2 September. Pronounced upslope of isotherms is seen between 390 and 320 nmi from the end of the section. The 25°C isotherm rises from 103 m to about 10 m within 30 nmi between 390 and 360 nmi from the end of the section. Similarly, the 20°C isotherm rises from 150 m to 70 m between 390 and 320 nmi from the end of the section. This pronounced upslope of isotherms occurs across the front between the equatorial and coastal water of the Great Whirl and the warm (T>26°C), saline (S>35.9 °/oo) water to the east that is of Arabian Sea origin. Sea surface salinities across this front decrease from 35.9 °/oo to 35.5 °/oo proceeding from east to west (figure 19). Between 320 and 200 nmi from the end of the section the isotherms exhibit a gradual slope downward toward the west. Within this horizontal distance of 120 nmi the 20°C isotherm deepens from 70 m to 140 m. The depth analysis of the 20°C isotherm (figure 30) indicates that this deepening of the isotherms is associated with the southeast corner of the Socotra Eddy. High sea surface salinities (S>35.8 °/oo) (figure 19) are collocated with the deepening isotherms in this area and thus are a further indication of the presence of water of Arabian Sea origin. Between 200 and 100 nmi from the end of the section a pronounced peaking of isotherms is observed. The 25°C isotherm breaks the surface between 140 and 160 nmi from the end, and the 20°C isotherm shoals from 140 to 60 m between 200 and 120 nmi from the end of the section. The minimum in the depth field of the 20°C isotherm (figure 30) reveals that this shoaling of isotherms is associated with the boundary between the Great Whirl and the Socotra Eddy. The last 120 nmi of this section is characterized by pronounced deepening of the isotherms. The 20°C isotherm deepens from 60 m to about 230 m for the last 120 nmi of the section. The analysis of the depth of the 20°C isotherm (figure 30) further reveals that this westward deepening of isotherms is connected with the anticyclonic center of the Great Whirl. Unfortunately, before the section could be completed with an approach to the coast, an employee became ill, and a direct track had to be steamed back to the Seychelles.

Section 10 (figure 15), taken from 2 to 4 September, was made to steam a direct track to the Seychelles. This section follows the southern half of the Great Whirl, as indicated by a sharp upward slope of isotherms to the south. It is interesting to note that the depth interval between the 24°C and 22°C isotherms decreases from 96 m at a location 500 nmi from the end of the section to 6 m at 250 nmi from the end of the section. The packing of isotherms along

this part of the section is an indication of shear along the southern boundary of the Great Whirl. Between about 2°N and 2°S, 260 and 40 nmi from the end of the section, isotherm spreading between the 25°C and 22°C isotherms was observed to increase from 40 to 120 m. This feature, which is characteristic of both the Atlantic and Pacific along the equator, indicates the presence of a shallow, easterly setting equatorial undercurrent (Neumann and Pierson, 1966). Although it is generally believed that the Equatorial Undercurrent in the western Indian Ocean is absent during the southwest monsoon (Neumann and Pierson, 1966; and Wyrtki, 1973), indications of its presence along section 10 may be explained by the relative weakness of the 1979 southwest monsoon and the lateness of the date of the observations, which were taken during the first week of September.

IV. WATER MASS ANALYSIS

Figures 16 and 17 show the sea surface bucket temperatures and salinities, respectively, for late June and early July 1979. Surface waters are in direct contact with the atmosphere, and temperature and salinity are not always sufficiently conservative at the surface to directly tag water masses. However, the currents in this area are sufficiently rapid to allow this. Salinity at the surface in this area is a better indicator than temperature of the nature and origin of the water.

From figures 16, 17, 18, and 19, it is possible to distinguish two distinctly different kinds of surface water in the Somali Basin. The fresher water with salinities less than 35.3 °/oo is advected into the Somali Basin by the South Equatorial Current from the eastern side of the Indian Ocean (Warren, et al., 1966). Such fresh water is the result of the excess of precipitation and river runoff over evaporation in the Bay of Bengal and the region of the Indonesian archipelago. Another much more localized source of relatively fresh water is the coastal upwelling induced by the prevailing southwesterly monsoons paralleling the Somali Coast. Such water can be readily identified by low temperatures (less than 22°C) accompanied by low salinities.

The second type of surface water, which is characteristic of the Socotra Eddy, found in this region is warm (>26°C) and saline (>35.6 °/oo). Its high temperature and salinity identify it as originating in the Gulf of Aden and the Arabian Sea, where evaporation exceeds precipitation and river runoff, and incoming solar radiation shows higher values than at any other location on the earth's surface (Sellers, 1965).

The complex intermingling of these two surface water masses can be seen in figures 16 and 17. The warm (>27°C), low-salinity (<35.3 °/oo) water straddling the equator off the Somali-Kenya coast originates in the South Equatorial Current and forms a clockwise rotating gyre called the Southern Eddy. This warm and relatively fresh water is separated from warm yet more saline (>35.5 °/oo) water by a ribbon of cold (<24°C), fresh (<35.1 °/oo) upwelled water located between 3°N and 5°N. The presence of two warm gyres south of Ras Hafun (10°N) is indicated in the XBT cross-section taken by the tankers AL DURIYAH and ESSO HONOLULU between 22°N and 2°S from 28 June to 3 July and 14-18 July 1979 (figures 20 and 21). Along these sections, two strong frontal zones centered at approximately 6°N and 10°N are apparent.

These two frontal zones are reflected in sea surface temperature minima situated near the coast and centered at approximately 5°N and 10°N (figure 16) and are indications of offshore flow at these latitudes. The TIROS-N satellite infrared image for 12 July 1979 (figure 22) also shows the two warm eddies and the two bands of cold upwelled water being advected offshore.

Figures 18 and 19 do not indicate the presence of a front between 3°N and 5°N. The broad area of low-salinity (<35.1 °/oo) water stretching along the coast from 3°N to about 10°N is the result of both the entrainment of comparatively fresh South Equatorial Current water into the Great Whirl and Ekman transport and entrainment of coastal upwelled water. The frontal zone between the Southern Eddy and Great Whirl breaks down during the rather short time of approximately ten days. The tanker section taken between 22°N and 2°S from 10 August to 17 August (figure 23) indicates a northward migration of the northern edge of the Southern Eddy of approximately 100 nmi from its observed position in late June and early July. An extremely well-formed Great Whirl off the Somali Coast between 5°N and 10°N is seen in the TIROS-N satellite infrared image for 18 August 1979 (figure 2). The Southern Eddy is unfortunately obscured by clouds but it is undoubtedly present owing to the pronounced ribbon of cold water on the southern edge of the Great Whirl.

The XBT cross-section taken by the ESSO CARRIBEAN from 25 to 31 August 1979 between 2°S and 22°N (figure 24) reveals a single front at 9°N separating two large warm eddies centered at approximately 5°N and 12°N. The Southern Eddy and Great Whirl had merged into a single warm anticyclonic eddy. In the TIROS-N satellite IR image for 27 August 1979 (figure 3), the front between the Southern Eddy and the Great Whirl has disappeared. The upwelled water off the coast between 9°N and 10°N seen in the image is manifested in the sharp peaking of isotherms in the ESSO CARRIBEAN cross-section at the same latitude. This cold upwelled water forms the southwestern edge of the Socotra Eddy.

The interplay between water masses of different origin is evident in temperature-salinity relationships from the STD stations taken in the area. The gross shapes of the temperature-salinity (T-S) curves (figure 25) in the area show only slight variation in salinity from the surface down to 1500 m. Although T-S curves in this region are encompassed by a fairly narrow salinity envelope, these curves are characterized by a rather ragged and irregular salinity structure in the layer between 200 m and 1000 m. Below the salinity minima and maxima of the intermediate layers (300 m - 800 m) the T-S curves between 800 m and 1500 m show remarkably uniform straight lines between the points T=10.0°C, S=35.4 °/oo and T=5.0°C, S=34.9 °/oo in the region of the Somali Basin. Some of this water (T>9°C) is from the Subtropical Convergence near latitude 40°S (Warren, et al., 1966). This water is too warm and too saline to be considered Antarctic Intermediate Water. Antarctic Intermediate Water with its strong salinity minimum (<34.65 °/oo) is obliterated by southward-flowing high salinity water from the northwestern Indian Ocean between 15°S and 5°S (Warren, et al., 1966).

The water which underlies the Subtropical Subsurface Water in the Somali Basin is the North Indian Deep Water whose upper limit is found on the 27.6 σ_t surface (T=6.5°C, S=35.1 °/oo) and is located at 1200 to 1300 m depth. Below 1300 m, salinity decreases monotonically with temperature until abyssal values of 1.3°C and 1.4°C are reached (Warren, et al., 1966). The smooth continuous

curve between the points T=10.0°C, S=35.4 °/oo and T=5.0°C, S=34.9 °/oo is evidence of pronounced mixing along isopycnal surfaces between these two water masses. Weak stratification between Subtropical Subsurface Water and North Indian Deep Water is indicated on a T-S diagram in which the curve of the two water masses parallels rather than crosses lines of constant σ_t. This lack of density stratification leads to strong mixing of two water masses of differing temperatures and salinities, yet similar densities. Oxygen concentrations could be a means to tag the Subtropical Subsurface and North Indian Deep Waters of the northwestern Indian Ocean. Owing to its origin in upper and middle latitudes of the southern Indian Ocean where it is subjected to storm-induced wind mixing, the former should have the higher concentration of dissolved oxygen.

At about 2500 m, the water in the Somali Basin is principally Antarctic Circumpolar Water originating in the broad band between the Antarctic and Subtropical Convergence (Warren, et al., 1966). The formation of this water explains the oxygen maximum which underlies the comparatively oxygen-poor North Indian Deep Water.

Although Warren, Stommel, and Swallow (1966) do not mention the presence of Antarctic Bottom Water in the Somali Basin, Lowrie (1980) is convinced that there is strong flow of this water into the Somali Basin. Antarctic Bottom Water, having bottom potential temperatures of less than 1°C, is formed along the coast of Antarctica, principally in the Weddell Sea. This water, underlying Antarctic Circumpolar Water, enters the northern part of the Indian Ocean by flowing along the eastern edge of the Madagascar Plateau into the Madagascar Abyssal Plain off the east coast of Madagascar. From the Madagascar Abyssal Plain, Antarctic Bottom Water enters the Somali Basin through the Amirante Passage between the Seychelles and the Farquhar Island Group north of Madagascar. The extreme depth of the Amirante Passage, which is in excess of 5000 m in some places, and the coarse grain sizes (Lowrie, 1980) found along the bottom, indicate considerable flow of Bottom Water through this opening. From the Amirante Passage, Antarctic Bottom Water is free to fan out onto the floor of the deep Somali Basin. The three deep stations taken on the first leg of the survey, station numbers 15 (8° 27.1'N, 51° 42.0'E), 20 (10° 16.3'N, 53° 29.7'E), and 22 (11° 04.8'N, 55° 53.9'E) revealed bottom potential temperatures of 0.97°C, 0.97°C and 1.12°C, respectively. Although these three stations taken in the northern part of the Somali Basin can hardly be considered conclusive proof of the existence of Antarctic Bottom Water in this area, the low bottom potential temperatures observed at these locations are in good agreement with previous measurements.

The first station (figure 25) taken at 0° 03.0'N, 50° 56.1'E, only three nmi north of the equator, shows a shallow, yet strong, salinity maximum between 50 m and 100 m. This salinity maximum, located as it is in an area of mass convergence, is the result of wind-driven transport of warm, saline water toward the equator. Since a similar salinity maximum occurs along the Atlantic equator and is associated very closely with the Atlantic Equatorial Undercurrent, this feature might be attributed to an Indian Ocean Equatorial Undercurrent. However, the Equatorial Undercurrent in the Indian Ocean is associated with the northeast monsoon and is absent during the southwest monsoon (Wyrtki, 1973). The lack of an Equatorial Undercurrent in the Indian Ocean during the southwest monsoon is explained by the thermohaline structure of the equatorial

Indian Ocean; warm, fresh water on the eastern side of the Indian Ocean in the region of the Indonesian Archipelago is responsible for larger steric anomalies off the coast of Sumatra than are to be found off the coast of Africa, thus causing a sea surface slope upward toward the east along the Indian Ocean equator. Because of the lack of an Equatorial Undercurrent and the comparative freshness of the near surface waters of the southern part of the Somali Basin, the presence of the shallow subsurface salinity maxima at stations 1 and 2 between 50 m and 100 m is unexpected. It may be explained by a mass influx of saline water from the south compensating for a depressed sea surface on the western side of the equatorial Indian Ocean.

Below the subsurface salinity maximum at station 1, the water freshens. With the exception of weak salinity minima at 125 m and 400 m, the T-S curve is quite smooth to 1500 m. The salinity minimum at 400 m is possibly the result of the advection of warm, fresh Pacific Equatorial Water westward by the South Equatorial Current from its formation area in the Banda Sea (Warren, et al., 1966). The fresh water between 800 m and 1500 m (S=35.00 °/oo to 34.85 °/oo) consists of remnants of Antarctic Intermediate Water overlain by Subtropical Subsurface Water.

Proceeding north and west into the Somali Basin toward the Somali Coast, the near surface salinity maximum disappears, and a salinity maximum appears between about 800 m and 1000 m depths. This salinity maximum, which is centered on the 27.3 σ_t surface, has been designated Red Sea Water and is prevalent throughout the Somali Basin (Fenner and Bucca, 1972). Although Red Sea Water covers a large geographical area, its effects are less pronounced in the Indian Ocean than those of the Mediterranean Intermediate Water in the Atlantic. Fenner and Bucca (1972) report that only 200 nmi east of the Strait of Bab el Mandeb, only 35% of the Red Sea Water remains unmixed. In contrast, more than 95% of the Mediterranean Intermediate Water was found unmixed 250 nmi west of the Strait of Gibraltar.

At stations 10 and 15 (figure 25), a shallower and much weaker salinity maximum was observed at the 26.6 σ_t surface. This is Persian Gulf Water which is warmer and lighter than Red Sea Water. Much less pronounced in its effects than Red Sea Water, Persian Gulf Water acquires its characteristics in the small, shallow Persian Gulf, which is characterized by a large excess of evaporation over precipitation and river runoff. Persian Gulf and Red Sea Waters are separated by a tongue of Subtropical Subsurface Water centered between the 26.7 σ_t and 26.8 σ_t surfaces (Warren, et al., 1966).

Station 10 (figure 25), located slightly south of the center of the Great Whirl at 5° 01.2'N, 51° 52.2'E, is an excellent illustration of the several water masses present in the northwestern Indian Ocean. From the surface down to 150 m this station shows nearly isohaline water of salinity between 35.0 °/oo and 35.1 °/oo. This water is fresh upwelled water transported offshore from the Somali Coast by southwesterly monsoon winds. The water at 200 m, showing a pronounced increase of salinity from 150 m to 200 m, is of local origin, as shown by its shallowness and low density. The next prominent feature at this station is the salinity maximum between 300 m and 400 m. At 334 m the salinity was measured at 35.41 °/oo at a σ_t value of 26.726, which is characteristic of Persian Gulf Water. At about 500 m, an intermediate salinity minimum is observed. This salinity minimum, centered about the 27.0 σ_t surface, is

Subtropical Subsurface Water. Immediately underlying this is another salinity maximum centered between the 27.2 σ_t and 27.3 σ_t surfaces. This water is Red Sea Water, found between the 27.2 σ_t and 27.3 σ_t surfaces and the 600 m and 800 m depths. Below 800 m, the T-S curve is nearly a straight line to 1500 m, indicating the presence of North Indian Deep Water centered between 1200 m and 1300 m at the 27.6 σ_t surface (S=35.1 $^{o}/_{oo}$, T=6.5^{o}C) (Warren, et al., 1966). Although North Indian Deep Water is formed in the northern part of the western Indian Ocean, it is strongly diluted by Antarctic Circumpolar Water and traces of Antarctic Intermediate Water.

Station 15 (8^{o} 27.1'N, 51^{o} 42.0'E) (figure 25) is located near the northwestern edge of the Great Whirl. Because this station is situated near a region of strong coastal upwelling, the near surface waters down to about 150 m are remarkably uniform in salinity. At 200 m a salinity maximum of about 35.4 $^{o}/_{oo}$ appears, overlying a weak salinity minimum at about 250 m, which in turn overlies a second salinity maximum at about 300 m. The two salinity maxima, located on the 26.4 σ_t and 26.8 σ_t surfaces, are the result of two tongues of Persian Gulf Water separated by an intermediate layer of fresher water. The pronounced salinity minimum at 400 m is not easily explained from salinity analyses alone. Although Banda Sea Water and Antarctic Intermediate Water could produce a salinity minimum at about 400 m, Warren et al. (1966) feel that Subtropical Subsurface Water, which is poorer in dissolved oxygen than Antarctic Intermediate Water, is responsible for the salinity minimum. Unlike the salinity minima in the Atlantic and Pacific, which occur together with the oxygen maxima, the salinity minimum in the Indian Ocean is separate from the oxygen maximum. From this, it is reasonable to infer that the intermediate salinity minimum in the Indian Ocean is not attributable to Antarctic Intermediate Water. The salinity maximum between 600 m and 800 m is Red Sea Water with a σ_t value of about 27.3. Below Red Sea Water at about 800 m, the T-S curve becomes quite smooth and uniform and is a nearly straight line down to 4000 m. Underlying the Red Sea Water is North Indian Deep Water whose upper limit is considered to be the 27.6 σ_t surface (S=35.1 $^{o}/_{oo}$, T=6.5^{o}C). Below about 2500 m are found Antarctic Circumpolar Water and Antarctic Bottom Water.

Station 22 (11^{o} 04.8'N, 55^{o}53.9'E) (figure 25), located about 200 nmi to the southeast of Socotra Island, is representative of the water found in the Socotra Eddy. The T-S curve for this station lacks the variable salinity structure found at stations taken further south and shows the influence of the warm, saline Arabian Sea as reflected in its pronounced rightward displacement. Persian Gulf Water is not evident at this station. Although there is an extremely weak salinity maximum between 250 m and 300 m, it is not associated with Persian Gulf Water which is centered at the 26.6 σ_t surface. Instead, this water with σ_t values between 26.3 and 26.4, is formed in the near-surface layers of the Gulf of Aden and the Arabian Sea; it is too light to be associated with the Persian Gulf. The weak salinity minimum situated at 600 m near the 27.1 σ_t surface is diluted Subtropical Subsurface Water. The water underlying this weak salinity minimum is Red Sea Water with a high saline core at about 800 m near the 27.3 σ_t surface. Below 800 m, the T-S curve is nearly coincident with the T-S curve at station 15. Water below about 800 m is North Indian Deep Water underlain by Antarctic Circumpolar and Bottom Waters.

Salinity stratification in the region of the Somali Current is complex yet much weaker than that found in the North Atlantic. The two intermediate salinity maxima in the northwestern Indian Ocean are weak compared with the intermediate salinity maximum found at a depth of about 1000 m between the 27.6 σ_t and 27.8 σ_t surfaces in the North Atlantic. The small volumes and surface areas of the Persian Gulf (6×10^3 km^3 and 239×10^3 km^2) and Red Sea (215×10^3 km^3 and 438×10^3 km^2) compared with the Mediterranean excluding the Black Sea (3701×10^3 km^3 and 2505×10^3 km^2) are reasonable explanations of the relative weaknesses of the salinity maxima in the Indian Ocean. Weak density stratification between Red Sea and Antarctic Intermediate Waters is also evident in that the two water masses have approximately the same σ_t values (27.2 - 27.3) in spite of their strongly differing temperatures and salinities. Between σ_t values of 26.4 and 27.0, interfingering of Persian Gulf and Subtropical Subsurface Water is observed (Warren, et al., 1966). Such interfingering is responsible for temperature inversions and sound channels (Fenner and Bucca, 1972).

Subsurface temperature analyses in the region of the Somali Current reveal the double-cellular circulation bounded by colder water on the western and eastern edges of the survey area. The ribbon of cold upwelled water between the Great Whirl and the Socotra Eddy is especially evident in the 100 m, 200 m, and 300 m temperatures (figures 27, 28, and 29). Cold upwelled water adjacent to the coast appears in all subsurface temperature analyses.

The analysis of the temperatures at 50 m (figure 26) gives a slight indication of the double-cellular circulation. The 24°C and 26°C isotherms lack the circular pattern found in the other temperature charts, yet the temperature maxima associated with the Great Whirl and the Socotra Eddy are discernible. The 22°C water centered at about 8°N latitude is cold upwelled water entrained between the two anticyclonic gyres. Cold upwelled water ($T<12$°C) is clearly evident adjacent to the coast between 9°N and 10°N latitude. Analysis of the temperature field at 50 m was made difficult by the normal variations of the mixed layer about this depth. Since the layer depth was underlain by a strong thermocline, normal variations in mechanical wind mixing resulted in highly variable temperatures at 50 m. Such variations masked to a large extent normal temperature variations caused by the gross circulation of the Somali Current System.

The analyses of the 100 m, 200 m and 300 m temperatures (figures 27, 28, and 29) each show the Great Whirl and Socotra Eddy to be the salient oceanographic features in the area. Low temperatures adjacent to the coast, especially between 9°N and 10°N, signify coastal upwelling. The temperature minimum between the Great Whirl and the Socotra Eddy was a result of the entrainment of cold upwelled water and was found in a zone of strong shear and turbulence. The strong horizontal temperature gradient east of the Great Whirl and the Socotra Eddy was clearly evident at 100 m, yet was not found at 200 m or 300 m. The lack of a strong horizontal temperature gradient at 200 m and 300 m in the eastern edge of the survey area was an indication that the zone of shear found there, although strong, was quite shallow. The 300 m temperature analysis, while still showing the double-cellular circulation of the Great Whirl and Socotra Eddy, reveals a considerably weaker horizontal temperature gradient than that found at 100 m or 200 m. The rapidly weakening horizontal temperature gradient with depth is consistent with the dynamics of a strong but shallow wind-driven current.

The depth analysis of the 20°C isotherm (figure 30) is an especially effective presentation. The 20°C isotherm, which is located near the top of the upper thermocline, is an excellent tracer of the vertical displacement of this thermocline. Because fronts are regions of strongly sloping isotherms, the vertical location of the thermocline is a reliable indicator of the positions of fronts and eddies. Two depth maxima of the 20°C isotherm are shown in figure 30. The 20°C isotherm breaks the surface off the Somali coast between 9°N and 10°N and is found at a depth of less than 100 m between the Socotra Eddy and the Great Whirl. The minimum in the depth of the 20°C isotherm persists in an elongated pattern between the Socotra Eddy and Great Whirl and a large anticyclonic eddy immediately to the east of the survey area.

The analysis of the depth of the 15°C isotherm (figure 31) shows the anticyclonic circulation of the two eddies together with the strong zone of shear between them. The zone of shear to the east of the two eddies is still evident, but not nearly as pronounced as it is at the level of the 20°C isotherm. The lack of a strong discernible pattern in the depth of the 15°C isotherm near the eastern edge of the survey area is further evidence of the shallowness (<200 m) of the strong currents observed there.

V. DYNAMIC HEIGHT ANOMALIES

The anomalies of the dynamic topography in dynamic centimeters of the surface relative to 1500 dbar are shown in figure 32. This figure, which is based on data taken from 27 STD stations during the last two weeks of August and the first week of September 1979, shows the double-cellular nature of the circulation in the region. The two anticyclonic cells centered at approximately 5°N, 53°E and 11°N, 56°E are indications of the presence and strength of the Great Whirl and Socotra Eddy, respectively. Cold upwelled coastal water, which is denser than the warmer offshore oceanic water, is the cause of the low in the dynamic topography between 9°N and 11°N just off the Somali coast. Cold upwelled water advected offshore is entrained between the Great Whirl and the Socotra Eddy, causing strong shear between these two anticyclonic gyres. The small, weak cyclonic cell south of the Socotra Eddy, indicated by the broken line, is a result of offshore entrainment of cold upwelled water.

The dynamic topography anomalies in dynamic centimeters of the surface with respect to 1000 dbar and 500 dbar shown in figures 33 and 34, respectively, both show the double-cellular pattern evident in figure 32. Their similarity in dynamic topography configuration shows that there is little relative geostrophic motion at either the 500 dbar or 1000 dbar surface with respect to 1500 dbar. The analysis of the dynamic height anomalies of the 500 dbar surface with respect to 1500 dbar (figure 35) shows a weak reversal from the surface circulation. The two anticyclonic gyres become cyclonic with depth, and the circulation adjacent to the coast of Somalia centered near 10°N becomes anticyclonic. This weak reversal is a further indication of the location of a reference level or level of no motion at a depth somewhat shallower than 500 dbar. To further determine a shallow level of no motion, the method of Defant (1961) of determining the difference in dynamic heights between pairs of adjacent stations was used. This method indicated a reference level situated between 300 dbar and 500 dbar for most of the station

pairs examined. During the summer of 1964, Swallow and Bruce (1966), using both directly measured current meter observations and geostrophic calculations, found a reversal of the northeasterly near surface currents at depth between 300 m and 400 m. Below this depth they found southwesterly currents.

VI. GEOSTROPHIC CURRENT AND SALINITY CROSS-SECTIONS

Figure 36 shows geostrophic currents along section 1 (cm sec^{-1}) calculated relative to 1500 dbar. Station 1 (00° 03.0'N, 50° 54.1'E) was omitted from the current section because of its proximity to the equator where geostrophy is indeterminate. Surface geostrophic currents setting northeastward in excess of 300 cm sec^{-1} were measured between stations 5 and 6. In the upper 100 m between station 5 and 6 currents are in excess of 200 cm sec^{-1}, yet decrease rapidly with depth; at 400 m the current is only 29 cm sec^{-1}. The strong current within 40 nmi of the coast results from cold, dense water adjacent to the coast and the attendant low steric anomalies. Because the zone of rapid northeasterly setting currents is confined to a narrow strip about 80 nmi in extent immediately adjacent to the Somali Coast, it is reasonable to attribute this coastal circulation to upwelling induced by prevailing southwesterly monsoon winds paralleling the coast. The TIROS-N Satellite infrared image for 18 August 1979 (figure 2), which is contemporaneous with Section 1, reveals a patch of cold upwelled water in the vicinity of station 6 (03° 56.7'N, 48° 07.6'E). Further offshore the current reverses and becomes southwesterly between stations 3 (2° 13.0'N, 49° 10.1'E) and 4 (3° 0.5'N, 48° 33.3'E). This southwesterly flow is associated with the southern edge of the Great Whirl and the northern edge of the Southern Eddy. Between station 2 (00° 56.8'N, 50° 02.0'E) and 3 the flow is again northeasterly-setting below 100 m indicating the northern edge of the Southern Eddy. It should be remembered that this section was taken when the Great Whirl and the Southern Eddy were merging.

The salinity analysis made from this section (figure 37) reveals a rather irregular and chaotic salinity field. Of particular interest is the shallow salinity maximum observed at stations 1 and 2 between 60 m and 120 m depth. Although a similar salinity maximum observed in the equatorial Atlantic is associated with the eastward-setting Equatorial Undercurrent, Bruce (1973a) found the shallow salinity maximum straddling the Western Indian Ocean equator during the southwest monsoon season to be coincident with westward-setting currents. This salinity maximum is seen to be associated with weak (10-20 cm sec^{-1}) southwesterly-setting geostrophic currents. This saline (S>35.50 °/oo) water centered about the 24.0 σ_t surface has its origin in the Arabian Sea which had been subjected to continuous strong winds for about three months. The southwest monsoon season is a season of cooling rather than heating at the sea surface owing to strong evaporative cooling induced by persistent southwesterly monsoon winds. Large areas of the Arabian Sea are subject to a net sea-air heat flux in excess of 400 cal cm^{-2} day^{-1} which exceeds the net radiation balance in the area. Colon (1964) calculated values for the net sea-air heat flux at 11° 30'N, 58° 30'E during June to be as high as 690 cal cm^{-2} day^{-1}. The salinity maximum (S>35.40 °/oo) at station 6 at 130 m depth probably results from entrainment of near-surface Arabian Sea water along the southern edge of the Great Whirl into the northeastward-setting coastal current.

The intermediate salinity maximum at station 5 between 500 m and 600 m depth is very weak (S=35.10 °/oo to 35.15 °/oo) and is centered about the 27.1 σ_t surface. It is Red Sea Water advected by very weak southwesterly-setting currents below 500 m. This salinity maximum is underlain by a second, slightly stronger (S>35.25 °/oo) salinity maximum at stations 3 and 4 between 700 m and 900 m depth. The stronger salinity maximum is likewise the result of entrainment of Red Sea Water into the deep southwesterly-setting currents below 500 m and is centered between the 27.2 σ_t and 27.3 σ_t surfaces. Between about 1000 m and 1500 m the salinity decreases steadily with depth. This water between about 1000 m and 1500 m has been termed by Warren et al. (1966) North Indian Deep water and has characteristics of Antarctic Circumpolar water which is found at the surface at about 50°S throughout the Southern Ocean. This water has a σ_t value of about 27.6.

Figure 38 shows geostrophic currents (cm sec^{-1}) relative to 1500 dbar along section 2. This section crosses the center of the Great Whirl and reveals the anti-cyclonic surface and near-surface circulation indicated in the dynamic topography charts (figures 32, 33, and 34). Northeasterly-setting currents are again strongest in the near-surface levels immediately adjacent the coast where cold coastal water produces the trough in the dynamic topography. Surface and near-surface geostrophic currents set northeasterly out to station 11 (5° 34.4'N, 53° 20.9'E). Between stations 11 and 13 (6° 17.1'N, 57° 38.9'E) the currents become southwesterly-setting down to 1500 m. Between stations 8 (4° 29.1'N, 49° 26.8'E) and 9 (4° 40.8'N, 50° 29.7'E) below 150 m the currents become southwesterly-setting indicating a change from the anti-cyclonic circulation in the upper layers of the Great Whirl to what appears to be cyclonic circulation in the lower layers. This reversal in circulation is suggested in the chart of the dynamic topography of the 500 dbar surface relative to 1500 dbar (figure 35).

The salinities associated with section 2 (figure 39) again indicate the extremely complex and irregular salinity structure of the upper and mid-depths of the northwestern Indian Ocean. There are essentially three subsurface salinity maxima evident along section 2, each associated with its own formation area. The shallowest salinity maximum (S>35.40 °/oo) is found between 100 m and 200 m and is centered about the very strong near-surface pycnocline between the 24.0 σ_t and 26.0 σ_t surfaces. This water originates in the near-surface layers of the Arabian Sea, an area of intense solar insolation, evaporation, and wind mixing. The next salinity maximum is found between 250 m and 400 m at stations 10, 11, 12, and 13. The water in this salinity maximum (S>35.30 °/oo) is centered between the 26.0 σ_t and 26.9 σ_t surfaces and is characteristic of water originating in the Persian Gulf. The deepest salinity maximum (S>35.25 °/oo) is most pronounced at station 10 and is centered at approximately 800 m depth. Being centered about the 27.3 σ_t surface, this water is characteristic of Red Sea Water.

Figure 40 presents geostrophic currents (cm sec^{-1}) along section 4 calculated relative to 1500 dbar. This section taken from 23 to 26 August 1979 was made to traverse the northern edge of the Great Whirl and to assess the area of maximum upwelling south of Ras Hafun. The currents in this section are northeasterly with the exception of weak southwesterly flow between stations 13 and 14. Owing to the long distance between stations 13 and 14 current values based on dynamic height differences between them are probably

not very realistic. As on the previous two sections, the strongest northeasterly-setting currents are found immediately adjacent to the coast where cold, upwelled coastal water produces a pronounced trough in the dynamic topography. The currents diminish in strength away from the Somali Coast. However, records of ship set and drift along this section indicate that there was a strong easterly component of the current at the surface that paralleled rather than crossed the section.

The salinity cross-section associated with section 4 (figure 41) is highly complex and irregular. Relatively fresh (S<35.10 °/oo) water predominates in the upper 100 m at stations 17, 16, 15, and 14. This water is advected eastward a considerable distance (about 250 nmi) off the Somali Coast along the northern edge of the Great Whirl. Between 80 nmi and 100 nmi east of station 14 a sharp surface salinity gradient is encountered which is also evident in figure 19 as the boundary between relatively fresh (S<35.1 °/oo) upwelled coastal water and relatively saline (S>35.6 °/oo) oceanic Arabian Sea water. Below the subsurface layers three intermediate salinity maxima are apparent, especially at station 14. The shallowest salinity maximum (S>35.40 °/oo) occurs between 300 m and 350 m depth at station 14 and is centered between the 26.7 σ_t and 26.8 σ_t surfaces. Although the salinity analysis connects this salinity maximum with the highly saline (S>35.50 °/oo) surface water east of station 14, the σ_t values of 26.7 to 26.8 associated with it suggest that the water may have originated in the Persian Gulf. Problems in the analysis are posed by the long distance separating stations 13 and 14. The next salinity maximum apparent at station 14 occurs between 500 m and 600 m depth and is centered about the 27.0 σ_t surface which is intermediate between Persian Gulf and Red Sea Waters. The deepest salinity maximum at station 14 (S>35.40 °/oo) is centered near 900 m depth about the 27.4 σ_t surface and is characteristic of Red Sea Water.

Figure 42 depicts the geostrophic currents (cm sec^{-1}) relative to 1500 dbar along section 5 and 6 taken from 26 to 29 August 1979. The currents in the near-surface layers are northeasterly-setting and quite weak (<20 cm sec^{-1}). The circulation in this area is chaotic and complex as indicated by the TIROS-N Satellite infrared image for 27 August 1979 (figure 3), and it is highly likely that the wide spacing of STD stations has aliased out important small scale features of the thermohaline structure in the area. Moreover, section 5 parallels rather than crosses the lines of constant dynamic height anomalies.

Figure 43 reveals the irregular salinity structure associated with sections 5 and 6 in the upper and middle depths. Again, several intermediate salinity maxima are apparent. A near-surface salinity maximum at station 18 (9° 42.4'N, 52° 03.4'E) is centered at about 70 m depth and the 25.9 σ_t surface. This salinity maximum breaks the surface along section 6 thus indicating that the formation area of this water lies in the high evaporation area of the Arabian Sea. The next salinity maximum (S>35.30 °/oo) is found at stations 18 and 19 (11° 14.8'N, 52° 31.7'E) between 200 m and 300 m depth. Being centered between the 26.5 σ_t and 26.9 σ_t surfaces this water exhibits characteristics of Persian Gulf Water. Station 21 (9° 21.0'N, 54° 33.0'E) is characterized by a strong (S>35.50 °/oo), deep (400 m to 600 m) salinity maximum. This water, owing to the depth and strength of the salinity maximum, most likely originates in the Red Sea. The deepest salinity maximum

(S>35.30 °/oo) is centered between 800 m and 900 m depth and the 27.3 σ_t and 27.5 σ_t surfaces and is also characteristic of Red Sea Water.

Sections 7 and 8, taken from 29 to 31 August 1979, were made to assess the structure of the Socotra Eddy. The geostrophic currents (cm sec^{-1}) calculated relative to 1500 dbar along these two sections are presented in figure 44. Between stations 21 and 22 (11° 0.4'N, 55° 53.9'E) westerly-setting currents down to about 1200 m are found with the strongest flow in the upper 100 m exceeding 30 cm sec^{-1}. This is the westerly flow associated with the southern edge of the Socotra Eddy. The strongest easterly-setting currents are found between stations 22 and 23 (13° 39.8'N, 56° 10.5'E) and in the near-surface layers are in excess of 30 cm sec^{-1}. This easterly flow is associated with the northern half of the Socotra Eddy. Section 8, comprising stations 23, 24 (11° 54.2'N, 57° 31.1'E), and 25 (9° 54.8'N, 59° 14.8'E), is characterized by weak (<10 cm sec^{-1}) easterly-setting surface and near-surface currents. The dyanmic topography charts of the area (figures 32, 33, and 34) indicate that section 8 parallels rather than crosses the northeastern edge of the Socotra Eddy.

The salinity analysis associated with section 7 and 8 is presented in figure 45. Like the previous salinity cross-sections, sections 7 and 8 reveal the complex and highly variable salinity structure of the upper and middle depths of the northwestern Indian Ocean. The high surface salinities (S>35.7 °/oo) along these two sections identify this area as a source of high salinity water. At stations 22 and 23 a salinity maximum (S>35.60 °/oo) is found at about 300 m depth centered between the 26.4 σ_t and 26.9 σ_t surfaces. This water is characteristic of Persian Gulf Water. Between 700 m and 800 m a deep salinity maximum (S>35.50 °/oo) is observed centered about the 27.3 σ_t and 27.4 σ_t surfaces. The water associated with this salinity maximum is characteristic of Red Sea Water.

Figure 46 shows geostrophic currents (cm sec^{-1}) along section 9 calculated relative to 1500 dbar. This section was taken along the southern edge of the Socotra Eddy and more nearly parallels than crosses the lines of constant dynamic height. The weak northerly flow (<10 cm sec^{-1}) between stations 25 and 26 (9° 07.3'N, 57° 03.0'E) results from the trough in the dynamic topography between the Socotra Eddy and Great Whirl (figure 32). Weak southerly flow is found between stations 26 and 27 (7° 34.6'N, 55° 10.3'E) resulting from the intermediate trough in the dynamic topography between the Socotra Eddy and Great Whirl. This section was taken across an area of cyclonic shear between these two eddies.

The salinity cross-section associated with section 9 (figure 47) reveals a general decrease of salinity with depth. The surface salinity maxima (S>35.80 °/oo) at stations 25 and 26 is characteristic of Arabian Sea surface water. At stations 25 and 26 salinity maxima (S>35.55 °/oo) is centered between 200 m and 300 m depth and the 26.6 σ_t and 26.7 σ_t surfaces. The depth of occurrence and σ_t values associated with these salinity maxima indicate that this water has originated in the Persian Gulf. The weak salinity maximum (S>35.45 °/oo) at station 26 is centered between 600 m and 700 m depth and the 27.2 σ_t and 27.3 σ_t surfaces. This indicates that the water has originated in the Red Sea.

VII. FRONTAL CROSSINGS

During the survey, numerous pronounced sea surface temperature changes, as measured by the hull-mounted shipboard thermometer, were observed. Such sea surface temperature changes are not readily apparent on the sea surface temperature analysis chart (figure 18) for two reasons. The temperature analysis is based on discrete hourly bucket temperatures rather than a continuous analog trace. Such discrete observations alias out the effects of strong horizontal temperature gradients, thus leaving unknown the exact location or nature of thermal discontinuities. The second difficulty with the sea surface temperature analysis arises from its small scale: it is simply impossible to present a feature only a few nautical miles in extent on such a small-scale chart. In order to present sea surface temperature changes in a meaningful way, the locations of each significant surface thermal discontinuity are plotted and labeled in figure 48. The analog traces are reproduced and presented in figures 48a, 48b, and 48c.

The first group of temperature traces (A, B, and C) is associated with the remnants of the Southern Eddy before its merger with the Great Whirl. Trace A is a result of the strong thermal boundary between cold upwelled coastal water and warm oceanic equatorial water at the southern edge of the Southern Eddy. Trace B is an indication of cold upwelled coastal water at the shoreward boundary of the Southern Eddy. The eastern boundary of the Southern Eddy is evident in trace C, which was made on 21 August 1979 just as the Southern Eddy and the Great Whirl were merging. This front is also seen in the strong salinity gradient depicted in figure 19. Traces F, Q, and R are associated with the Great Whirl. The northern edge of the Great Whirl is evident in traces F and Q, while R is an indication of strong shear and turbulence near the center of the Great Whirl. The extemely strong upwelling in the area north of the Great Whirl adjacent to the coast south of Ras Hafun is indicated in traces G, H, I, and J. The boundaries of the Socotra Eddy are reflected in traces K, L, M, and P. The southern boundary of the Socotra Eddy is indicated by traces K and L. For ease of presentation, the orientation of trace L has been reversed. That is to say, the cold water on the right hand side of the trace is located south of the warm water on the left hand side. Traces M and P are crossings of the northern and eastern edges, respectively, of the Socotra Eddy. The thermal boundaries apparent in traces D, E, N, and O indicate the presence of the shear zone between the Socotra Eddy and Great Whirl and a large anticyclonic gyre to the east of the survey area. The use of continuous analog sea surface temperature traces makes it possible to determine immediately when a thermal discontinuity is crossed. For this reason, the shipboard hull-mounted thermometer is of great value in pinpointing the exact locations of frontal boundaries.

VIII. XBT FAILURES

Approximately 300 nmi from the Somali Coast along section 1 many XBT malfunctions occurred. Since there are numerous causes of XBT failures (Blumenthal and Kroner, 1977), T-4 and T-7 probes from several batches were launched to investigate the possibility of malfunctions being caused by a defective lot of probes. Examination of the analog traces produced from several batches of XBT probes revealed wire breakage between the bottom of

the upper thermocline (about 150 m depth) and 700 m. The similarity of the nature of these failures suggests that they resulted from a common cause rather than from random factors such as sea state, wire insulation penetration, manufacturing defects, and electrical interference. Since the region of the Somali Current during the southwest monsoon is characterized by strong current shear, it seems reasonable to ascribe the persistent wire failure to strains induced by the strongly shearing currents. The sea surface analog trace was examined, and it was found that the area of high XBT failure rate coincided with the strong sea surface temperature gradient associated with trace A (figure 48a). Similarly, this area of frequent XBT failures coincided with the strong sea surface salinity gradient encountered on section 1 (figure 19). Almost every other encounter with strong sea surface temperature and salinity gradients produced high XBT failure rates. The locations of XBT failures are plotted in figure 49.

IX. INTENSE DIURNAL HEATING

Trace S (figure 48c), made during the afternoon of 3 September 1979, resulted not from a frontal crossing but from intense solar insolation of the upper few meters of the water column, often termed the "afternoon effect". The wind was calm, and the sea surface was characterized by alternating bands of slick and capillary waves accompanied by a 2- to 3-foot swell. The spikes seen on trace S indicate a highly variable sea surface temperature field. It was found that the spikes on the sea surface temperature trace corresponded to the bands of slick or glassy sea surface, while the minima were encountered in the bands of capillary waves. Alternating bands of smooth glassy water and capillary waves are quite common in tropical and subtropical waters under calm or nearly calm conditions. Although the mechanisms for the formation of these alternating bands are not completely understood, Roll (1965) has proposed internal waves and subsurface convective cells as possible causes of their formation.

While transiting trace S between 300 and 280 nmi from the end of section 10, sea surface bucket temperatures of 30.9°C, 31.0°C, 30.4°C, and 30.1°C were observed. In spite of these extremely high surface temperatures, the XBT analog traces registered sea surface temperatures of only 28°C. These low readings were probably caused by the thermal lag of the thermistor in the nose of the XBT probe as it fell through the extremely shallow layer of warm surface water. To test this hypothesis, a styrofoam jacket was made for an XBT probe to give it a very low sink rate. The resulting XBT record, after being corrected for the low sink rate by comparison with a normal XBT drop (Bruce and Firing, 1974), showed a very thin layer -- less than 2 m -- of warm water, apparently caused by intense solar insolation accompanied by a lack of wind mixing.

X. DISCUSSION AND CONCLUSIONS

Although there is a definite consensus among meteorologists and oceanographers as to the existence of a causal link between the southwest monsoon winds and the Somali Current, it is not sufficient to attribute this current solely to local wind forcing. The wind induced coastal upwelling evident in satellite

imagery and shipboard hydrographic sections is significant but does not explain the rapidly setting (300 to 350 cm sec^{-1}) surface and near-surface currents and the extraordinarily large values of mass transport. Swallow and Bruce (1966) calculated geostrophic volume transports of 47.5 sverdrups in the upper 200 m relative to 1000 dbar along a hydrographic section offshore from the Somali Coast at 8°N during the 1964 southwest monsoon season. Direct current measurements along the same hydrographic section indicated volume transports of 62.4 sverdrups in the upper 200 m. The measured volume transports during the 1964 southwest monsoon season were found to be supergeostrophic.

In order to understand the dynamics of the Somali Current it is important to examine the relative importance of the local and remote forcing. In examining the effects of the low level Somali jet, Anderson and Rowlands (1976) showed the initial relative predominance of the local forcing of the prevailing strong southwesterly monsoon winds. In using nonlinear theory to preclude excess leakage of energy equatorward via the Kelvin wave, it was determined that the important feature of the local forcing mechanism was the longshore component of the wind stress. The longshore component of the wind stress is the explanation of the coastal upwelling along the Somali Coast and the accompanying geostrophic northward currents. The northward flow is initially propagated equatorward via the Kelvin wave, but as the local northward current builds up, the equatorward propagation is inhibited and the Kelvin wave is slowed down. This serves to amplify the effects of the local wind stress by preventing leakage of current energy into the equatorial Kelvin wave. The remote forcing of the Somali Current is provided by the wind stress field over the interior of the Indian Ocean. The effects of this remote wind stress field are propagated westward along the equator by equatorial Kelvin waves with the first baroclinic mode arriving at the Somali Coast in nine days. For this reason the effects of the local wind stress are much more immediate than those of the wind stress curl over the interior of the Indian Ocean (Anderson and Rowlands, 1976).

Although the volume transport of the fully developed Somali Current south of Socotra Island is approximately 70 sverdrups and is thus comparable to that found in the Gulf Stream, the Somali Current exhibits a strong increase in volume transport downstream. This increase is particularly dramatic between 0.5°N and 2.5°N with an increase from 13 to 30 sverdrups calculated from hydrographic sections taken during the 1964 southwest monsoon season (Düing, 1978). Although one might be led to ascribe this pronounced increase in mass transport to the local wind forcing of the southwest monsoon, the area between 0.5°N and 2.5°N is too close to the equator to contain the strong southwesterly monsoon winds prevalent along the central and northern Somali Coast. Moreover, there is no surface current during the southwest monsoon season in this area to supply the water required for the increase in volume transport.

The rapid increase in volume transport of the Somali Current raises the broader question of the water budget of the Somali Current/Arabian Sea circulation system in general. If the rapid increase in volume transport in the southern part of the Somali Current is caused by neither locally wind-induced upwelling nor a strong westerly-setting equatorial current, then one must ask, "Where does the water come from?" A more complete quantitative understanding of the quantities of water recirculated in the large anticyclonic eddies and advected into the Arabian Sea must be achieved. The exchange rates of water

between the anticyclonic eddies of the Somali Current system and the Arabian Sea are especially important owing to the summer cooling caused by wind mixing and evaporation accompanied by strong solar radiation in the Arabian Sea (Düing, 1978). The advection of comparatively fresh (S<35.1 °/oo) equatorial water from the Bay of Bengal and the Indonesian archipelago is also imperfectly understood. The broad patch of relatively fresh water encountered off the Somali Coast during the 1979 southwest monsoon season appears to be too extensive to be attributable solely to wind-induced coastal upwelling and the attendant offshore Ekman transport. The entrainment of comparatively fresh (S<35.1 °/oo) equatorial water into the southern edge of the Great Whirl is a likely explanation of this large patch of low salinity water extending almost 300 nmi from the coast.

Not only does the Somali Current disappear and even reverse during the northeast monsoon season, but there are significant variations from one southwest monsoon season to the next. Each southwest monsoon season is characterized by the development of a Great Whirl or Prime Eddy between about 4°N and 12°N in the Somali Basin. All oceanographic measurements known to this author taken during each southwest monsoon season studied reveal divergence of the northeastward-setting coastal current from the coast between 9°N and 10°N just south of Ras Hafun. This area south of Ras Hafun is the scene of particularly strong coastal upwelling, and it is the source region of the cold water separating the warm anticyclonic Great Whirl from the smaller (about 200 nmi in diameter) anticyclonic Socotra Eddy southeast of Socotra Island. Although the Great Whirl and the Socotra Eddy appear to be common to all southwest monsoon seasons, strong coastal upwelling also occurs at 4°N to 6°N during some, but not all southwest monsoon seasons. This second area of strong coastal upwelling is associated with a strong coastal current turning offshore at about 5°N which forms a boundary between the Great Whirl and a southern eddy centered between the equator and 4°N. During 1970 (Bruce, 1973) and 1976 (Bruce, 1979), the Southern Eddy formed and was separated from the Great Whirl by a band of cold, coastal upwelled water originating off the Somali Coast between 4°N and 6°N. During 1975, 1977, and 1978 a well developed Southern Eddy was not observed (Bruce, 1979). The early part of the 1979 southwest monsoon season was characterized by the formation of the Southern Eddy but NOAA TIROS-N satellite infrared imagery taken 18 August and 27 August 1979 revealed coalescence of the Southern Eddy and the Great Whirl in only nine days.

The explanations of the variations in circulation from one southwest monsoon season to the next are not clear. Bruce (1978) in tabulating mean meridional and zonal wind stress values of Marsden squares 066, 067, and 031 for June, July, and August during each year from 1947 to 1972 found that wind stress components may vary by a factor of two from year to year. It thus seems reasonable to surmise some correlation between wind stress values and the eddy configuration of the Somali Current System. Anderson and Rowlands (1976) suggest that year to year variability in the Somali Current region may be explained by slight changes in the positions and intensities of the forcing functions.

Future work in the area of the Somali Current and Arabian Sea is required during all seasons in order to assess the effects of seasonally varying wind stress components on the circulation in the area. Field work should involve

the coordinated use of survey ships, aircraft, and satellites with the maximum use of expendable instrumentation. The use of expendable instrumentation from both survey ships and aircraft facilitates coverage of the largest possible area in the shortest possible time. Expendable Current Profilers (XCPs) would provide extremely useful information on the current shear in the upper layers of the Somali Current system. Further work on theoretical models is also needed in order to explain the reasons for the behavior of the Somali Current/Arabian Sea circulation system.

REFERENCES

Anderson, D.L.T. and P.B. Rowlands, The Somali Current response to the southwest monsoon: the relative importance of local and remote forcing, Journal of Marine Research, 34(3), 395-417, 1976.

Beller, J.W., W.R. Curtis, and H. Iredale, Standard procedures for collecting and processing SVSTD data, Unpublished Manuscript, U.S. Naval Oceanographic Office, Bay St. Louis, MS, 1975.

Blumenthal, B.P. and S.M. Kroner, Guide to common shipboard expendable bathythermograph (SXBT) recording malfunctions, Technical Note 3700-75-77, U.S. Naval Oceanographic Office, Bay St. Louis, MS, 1977.

Bruce, J.G., Eddies off the Somali coast during the southwest monsoon, Journal of Geophysical Research, 84, 7742-7748, 1979.

Bruce, J.G., Equatorial undercurrent in the western Indian Ocean during the southwest monsoon, Journal of Geophysical Research, 78, 6386-6394, 1973a.

Bruce, J.G., Large-scale variations of the Somali Current during the southwest monsoon, 1970, Deep-Sea Research, 20, 837-846, 1973.

Bruce, J.G., Spatial and temporal variation of the wind stress off the Somali coast, Journal of Geophysical Research, 83, 963-967, 1978.

Bruce, J.G. and E. Firing, Temperature measurements in the upper 10 m with modified expendable bathythermograph probes, Journal of Geophysical Research, 79, 4110-4111, 1974.

Colborn, J.G., The Thermal Structure of the Indian Ocean, University of Hawaii Press, Honolulu, 173 pp., 1975.

Colon, J.A., On interactions between the southwest monsoon current and sea surface over the Arabian Sea, Indian Journal of Meteorological Geophysics, 15, 185-200, 1964.

Defant, A., Physical Oceanography, Vol. I, Pergamon Press, New York, 729 pp., 1961.

Düing, W., The Monsoon Regime of the Currents in the Indian Ocean, University of Hawaii Press, Honolulu, 68, 1970.

Düing, W., The Somali Current: past and recent observations, Review Papers of Equatorial Oceanography FINE Workshop Proceedings, Scripps Institution of Oceanography, La Jolla, CA, June 27-August 12, 1977, 1978.

Düing, W. and K.H. Szekielda, Monsoonal response in the western Indian Ocean, Journal of Geophysical Research, 76, 4181-4187, 1971.

Fenner, D.F. and P.J. Bucca, The sound velocity structure of the North Indian Ocean, Technical Report 231, U.S. Naval Oceanographic Office, Bay St. Louis, MS, 1972.

Hurlburt, H.E. and J.D. Thompson, A numerical model of the Somali Current, Journal of Physical Oceanography, 6, 646-664, 1976.

Leetma, A., The response of the Somali Current at 2°S to the southwest monsoon of 1971, Deep-Sea Research, 20, 397-400, 1973.

Leetma, A., The response of the Somali Current to the southwest monsoon of 1970, Deep-Sea Research, 19, 319-325, 1972.

Lighthill, M.J., Dynamic response of the Indian Ocean to onset of the southwest monsoon, Philosophical Transactions of the Royal Society of London, A 265, 45-92, 1969.

Lowrie, A., Personal communication, 1980.

Neumann, G. and W.J. Pierson, Principles of Physical Oceanography, Prentice-Hall, Inc., Englewood Cliffs, NJ, 545 pp., 1966.

Roll, H.U., Physics of the Marine Atmosphere, Academic Press, New York, 426 pp. 1965.

Sellers, W.D., Physical Climatology, University of Chicago Press, Chicago, 272 pp., 1965.

Stommel, H.M., The Gulf Steam, A Physical and Dynamical Description, University of California Press, Berkeley and Los Angeles, CA, 248, 1965.

Swallow, J.C. and J.G. Bruce, Current measurements off the Somali coast during the southwest monsoon of 1964, Deep-Sea Research, 13, 861-888, 1966.

Warren, B., H.M. Stommel, and J.C. Swallow, Water mass and patterns of flow in the Somali basin during the southwest monsoon of 1964, Deep-Sea Research, 13, 825-860, 1966.

Wyrtki, K., An equatorial jet in the Indian Ocean, Science, 181, 262-264, 1973.

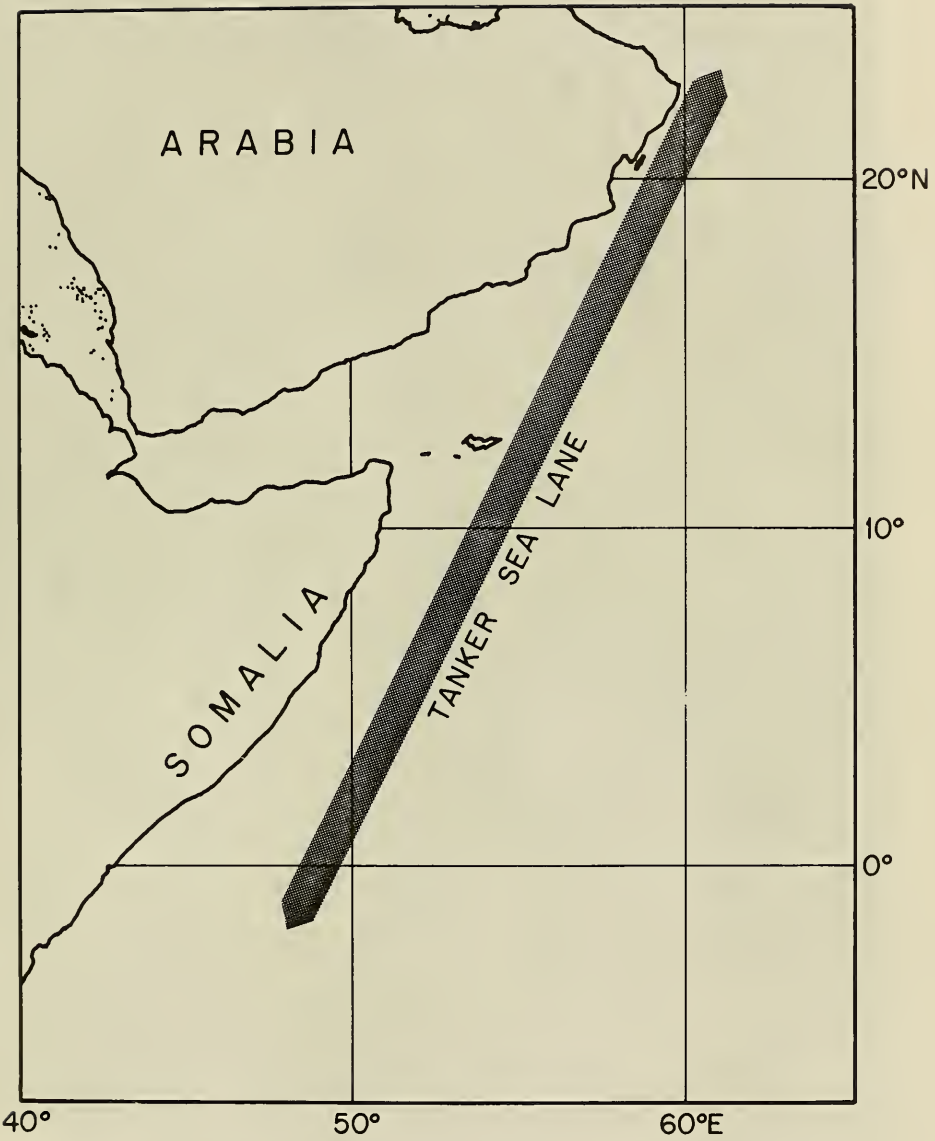

Figure 1. Location of sea lane transited by EXXON tankers taking time-series XBT's (Bruce, 1978)

Figure 2. Satellite imagery for 2356Z, 18 August 1979, NOAA 4, Orbit 4352, VHRR

Figure 3. Satellite imagery for 0001Z, 27 August 1979, NOAA 4, Orbit 4479, VHRR

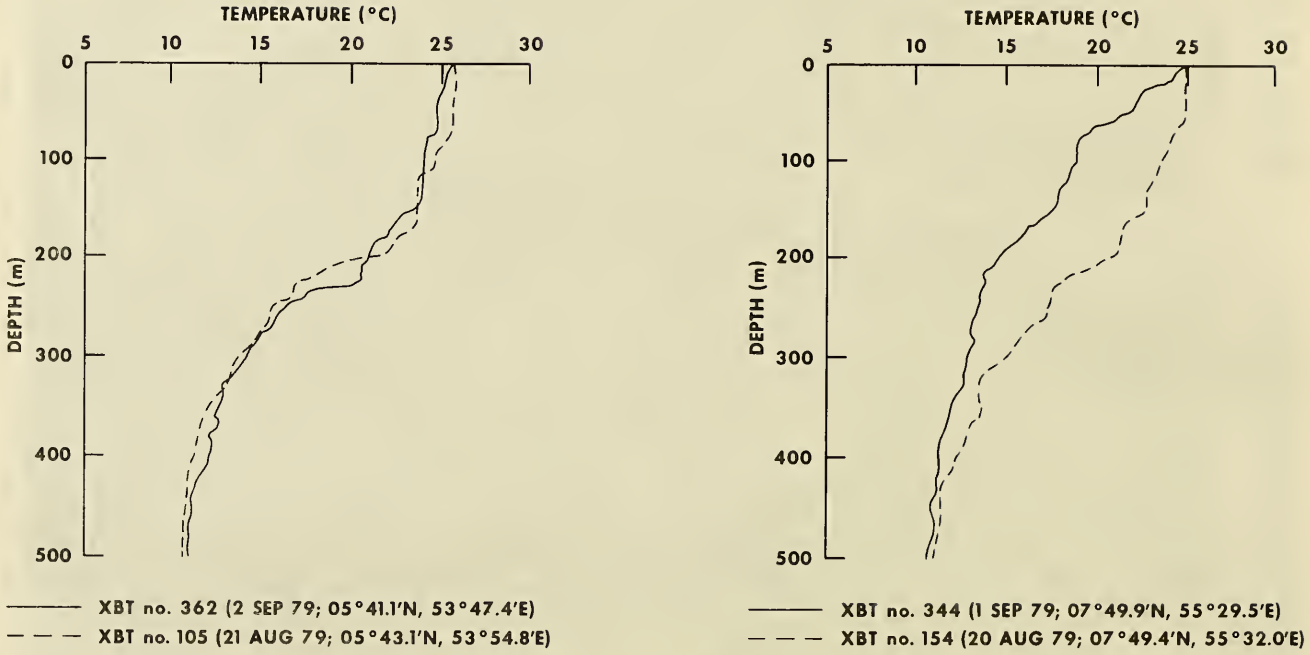

Figure 4. XBT profiles at approximately same station position 12 days apart

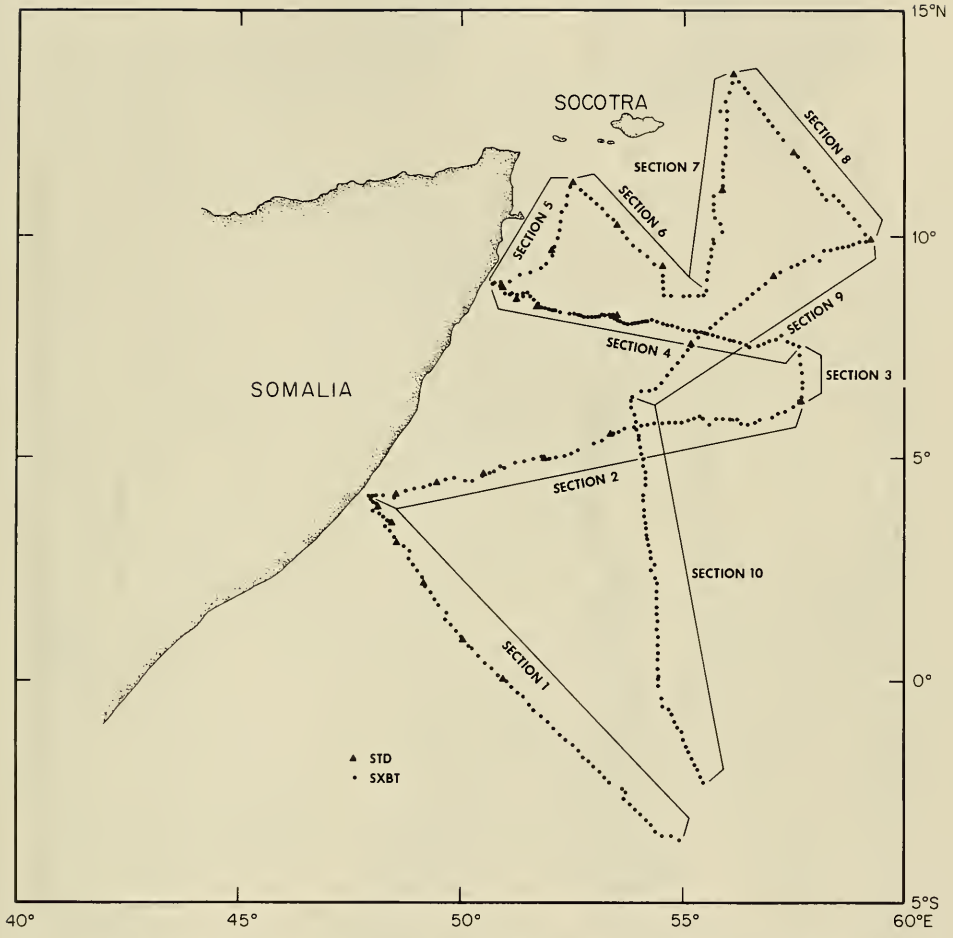

Figure 5. XBT and STD station positions, USNS WILKES, 16 August - 5 September 1979

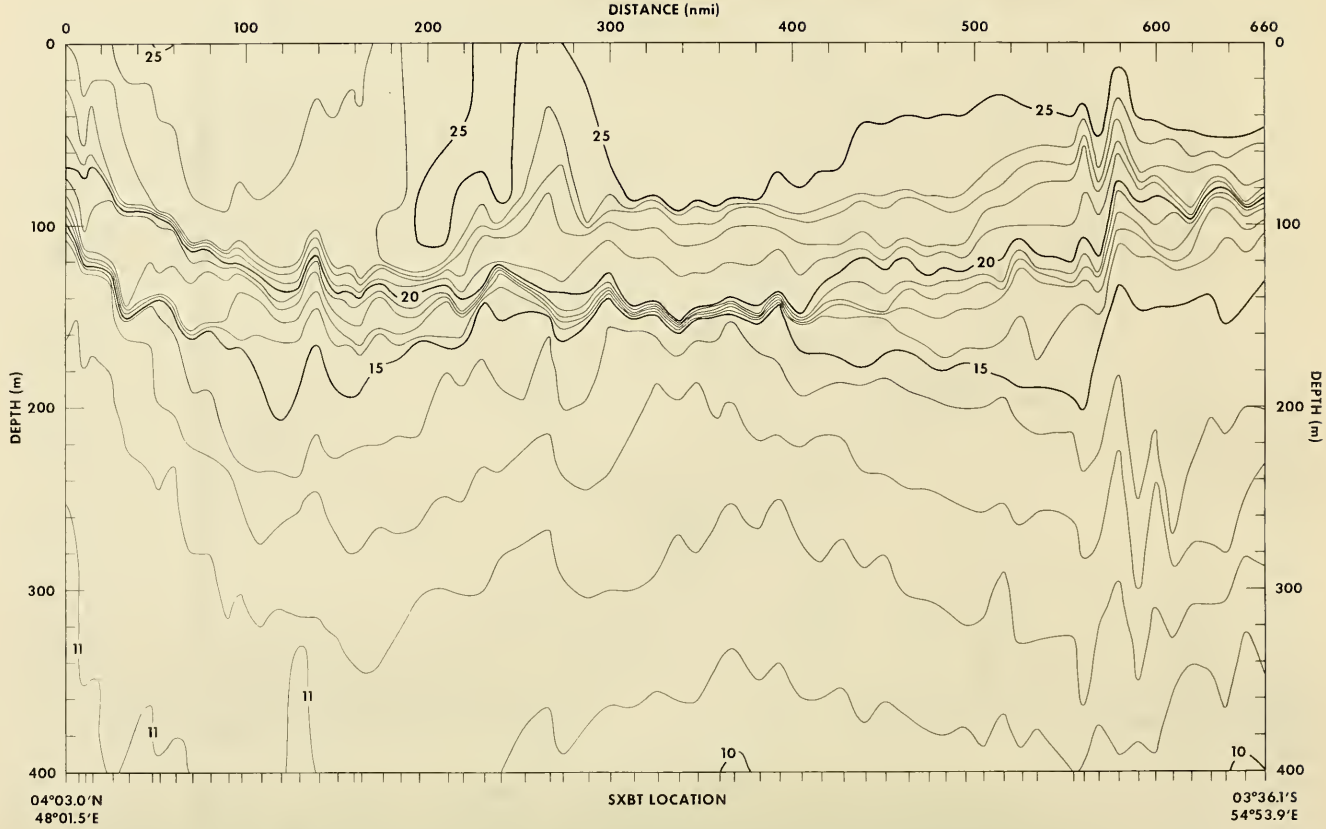

Figure 6. XBT Temperature (°C) Section 1, 16 - 19 August 1979 (see figure 5)

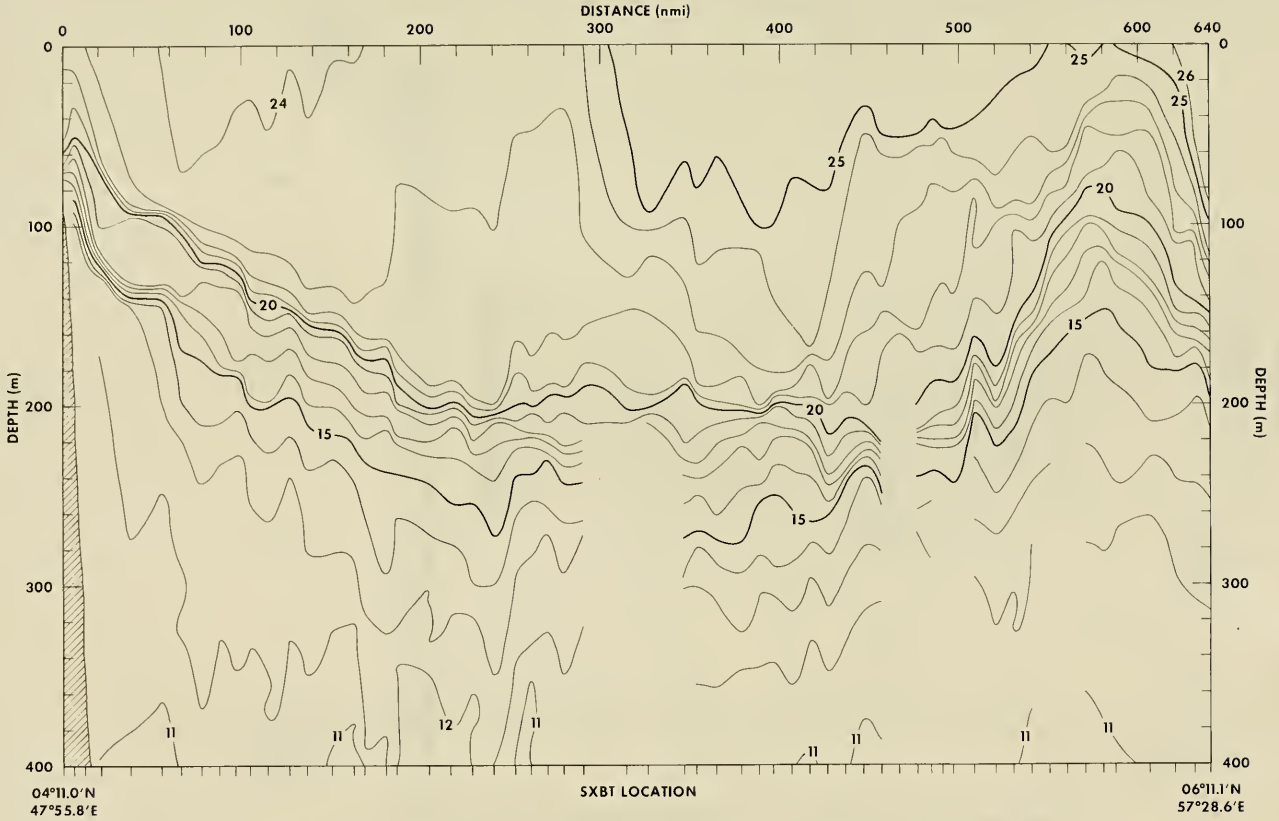

Figure 7. XBT Temperature (°C) Section 2, 19 - 22 August 1979 (see figure 5)

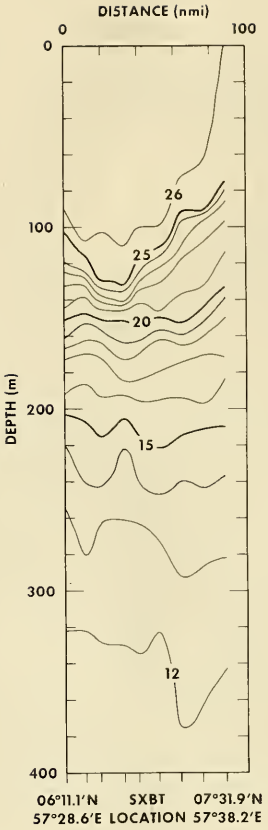

Figure 8. XBT Temperature (°C) Section 3, 22 - 23 August 1979 (see figure 5)

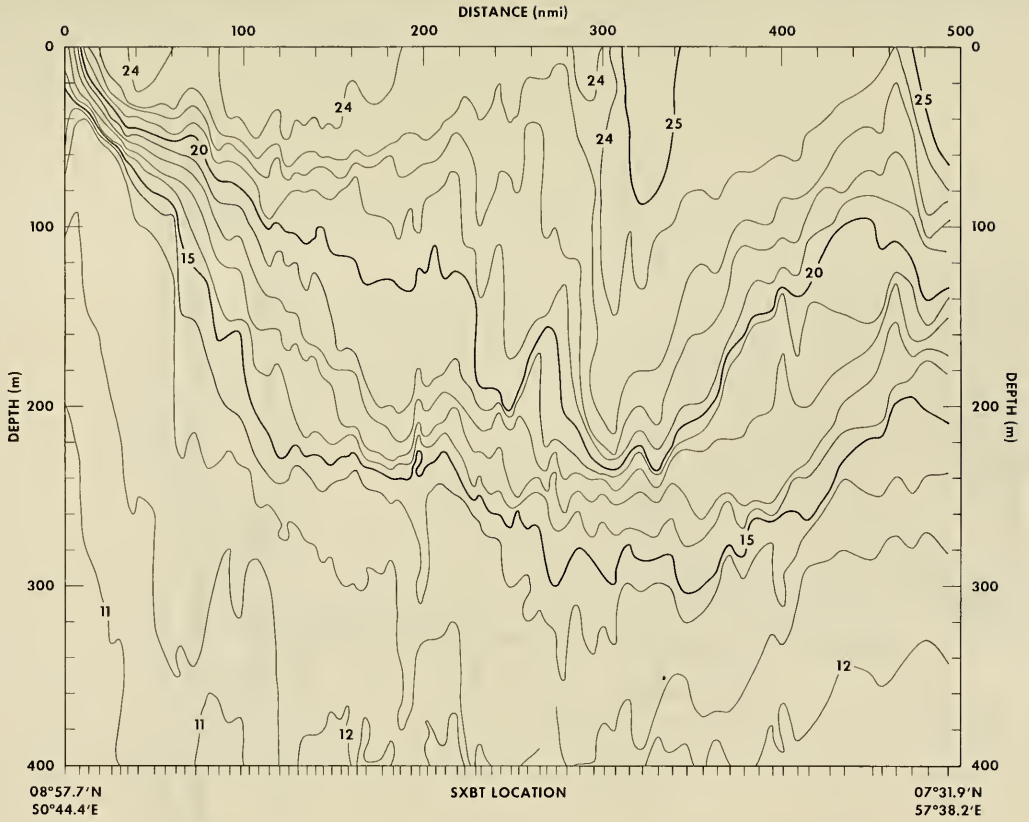

Figure 9. XBT Temperature (°C) Section 4, 23 - 26 August 1979 (see figure 5)

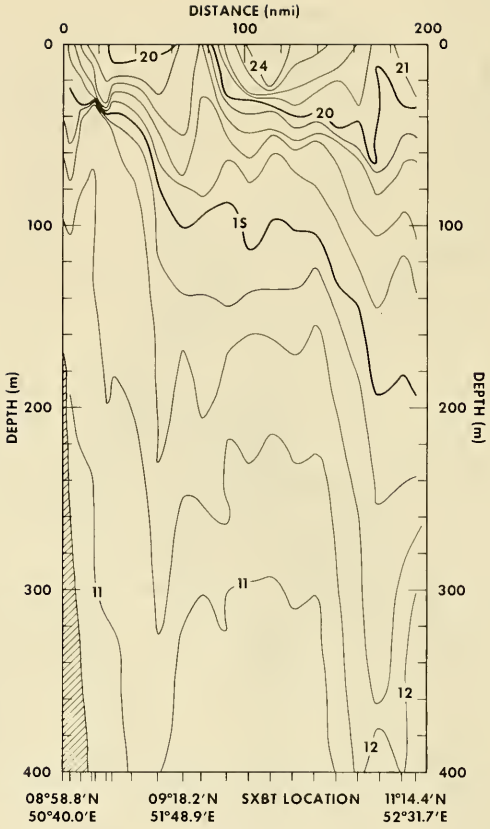

Figure 10. XBT Temperature (°C) Section 5, 26 - 27 August 1979 (see figure 5)

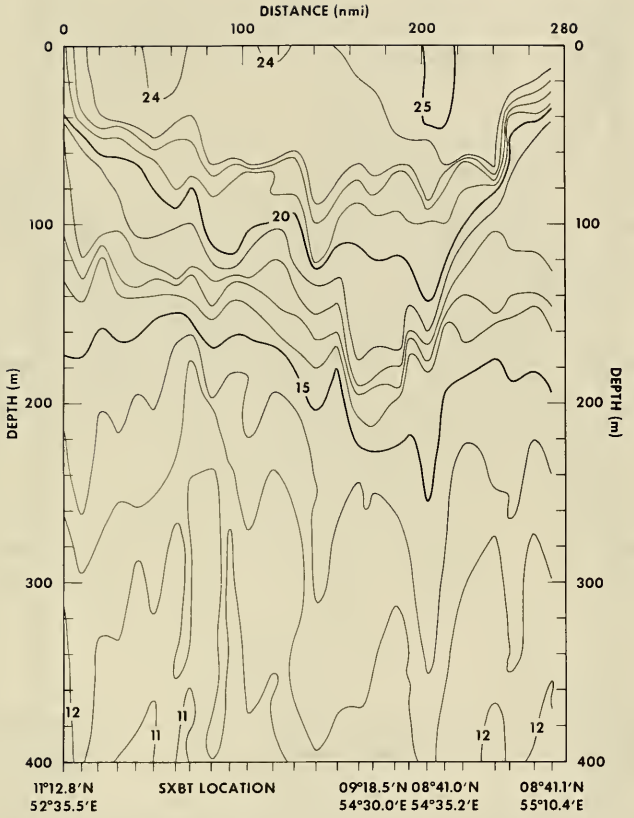

Figure 11. XBT Temperature (°C) Section 6, 27 - 28 August 1979 (see figure 5)

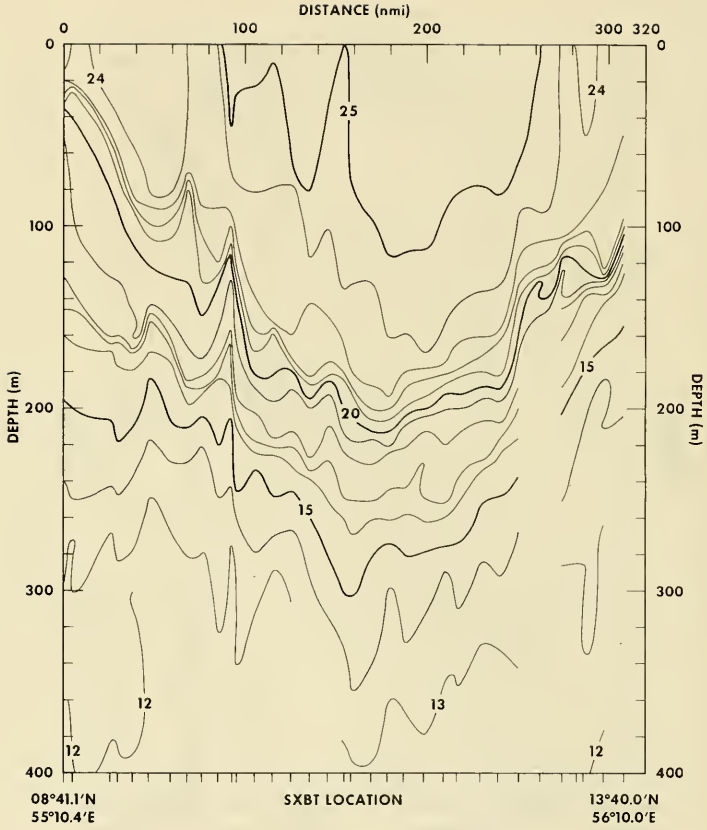

Figure 12. XBT Temperature (ºC) Section 7, 28 - 30 August 1979 (see figure 5)

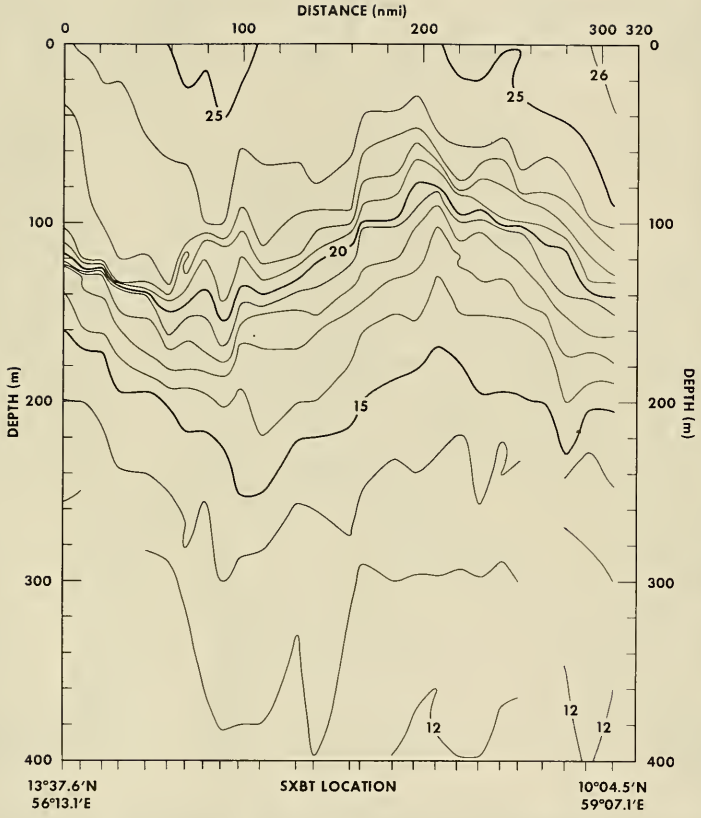

Figure 13. XBT Temperature (°C) Section 8, 30 - 31 August 1979 (see figure 5)

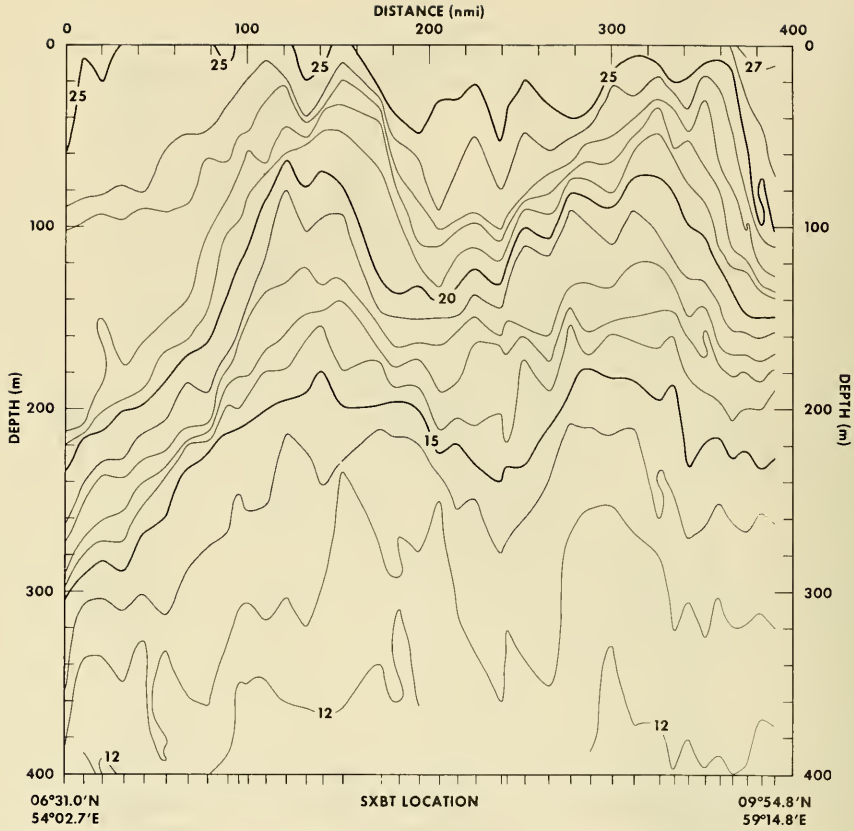

Figure 14. XBT Temperature (°C) Section 9, 31 August - 2 September 1979 (see figure 5)

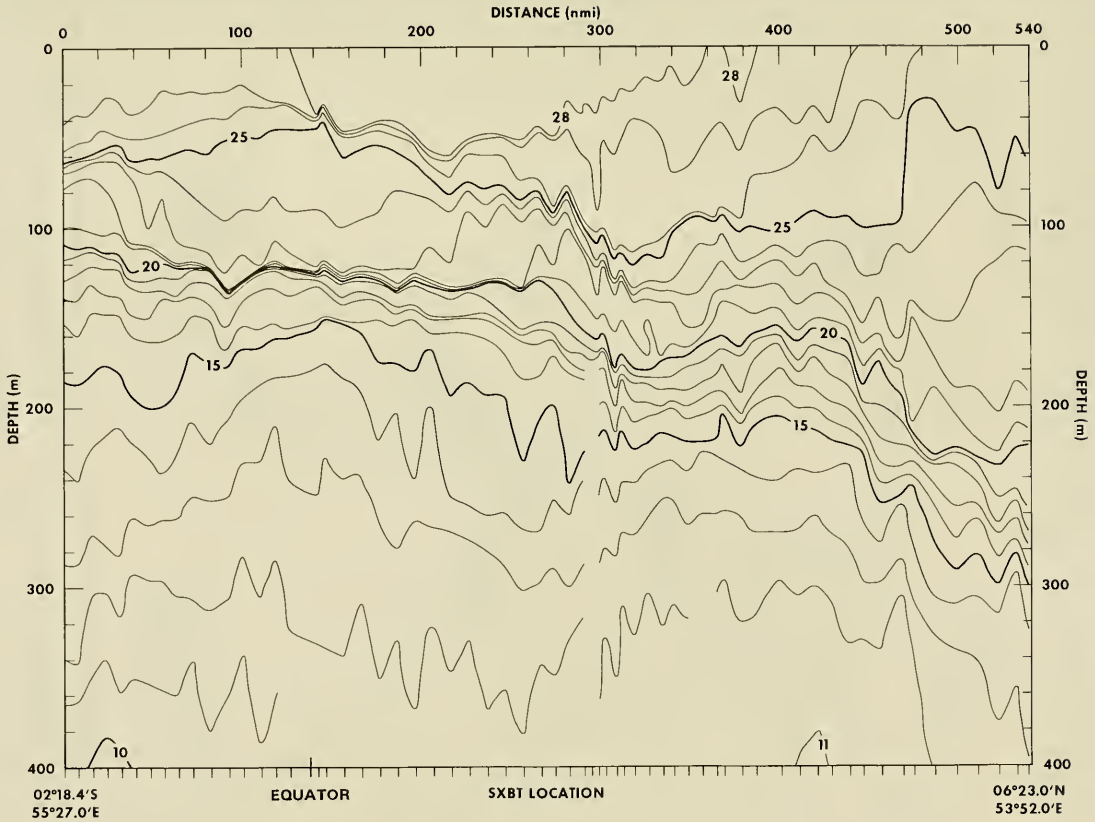

Figure 15. XBT Temperature (°C) Section 10, 2 - 4 September 1979 (see figure 5)

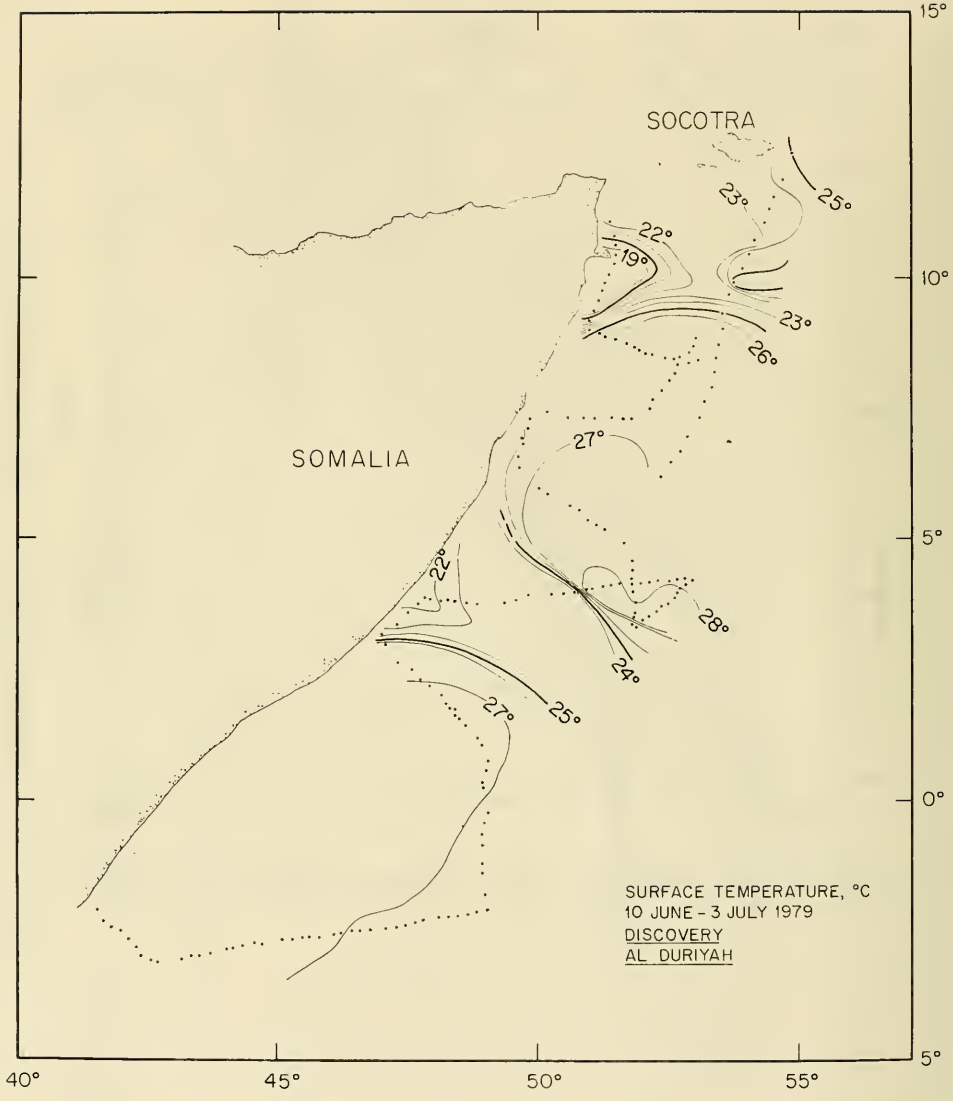
SOCOTRA
SOMALIA
25°
23°
22°
19°
23°
26°
27°
22°
28°
24°
27°
25°
SURFACE TEMPERATURE, °C
10 JUNE - 3 JULY 1979
DISCOVERY
AL DURIYAH
15°
10°
5°
0°
5°
40°
45°
50°
55°

Figure 16

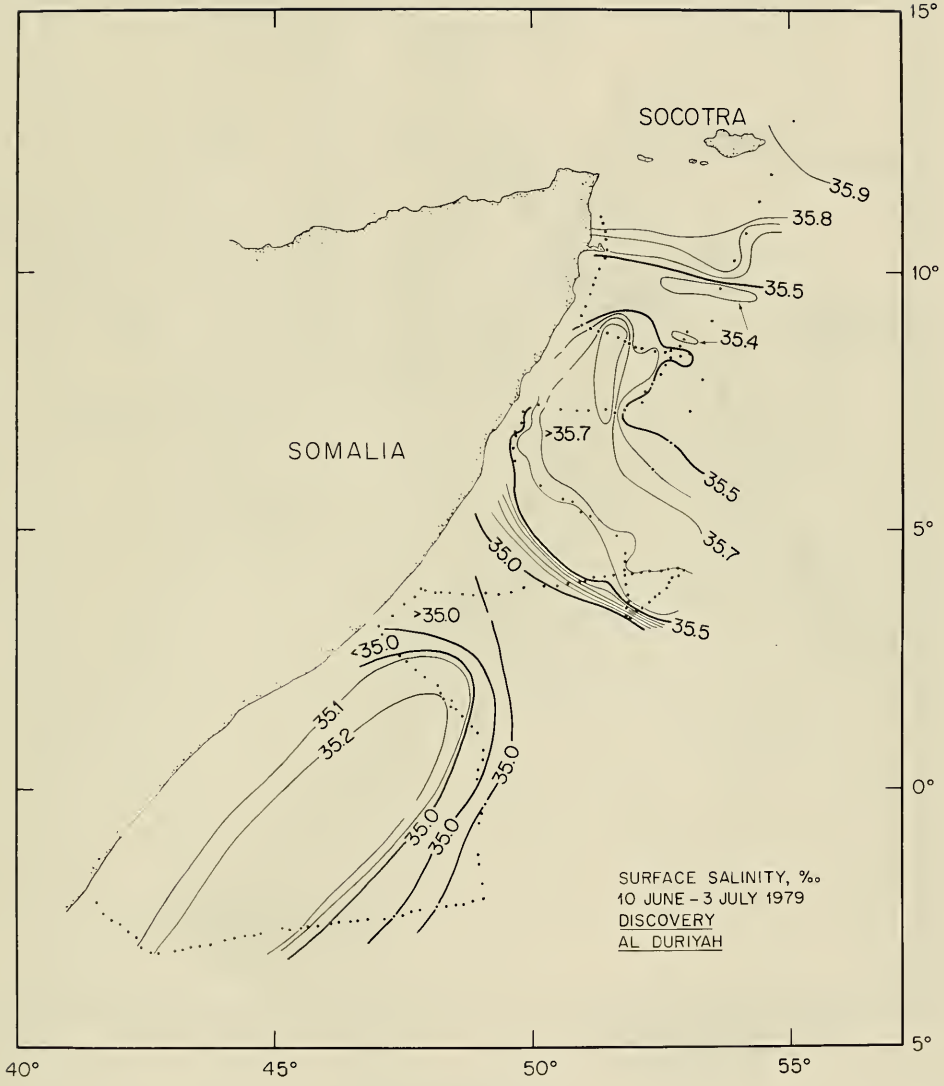
SOCOTRA
SOMALIA
35.9
35.8
35.5
35.4
>35.7
35.5
35.7
35.0
35.5
>35.0
<35.0
35.1
35.2
35.0
35.0
35.0
15°
10°
5°
0°
5°
40°
45°
50°
55°
SURFACE SALINITY, ‰
10 JUNE - 3 JULY 1979
DISCOVERY
AL DURIYAH

Figure 17

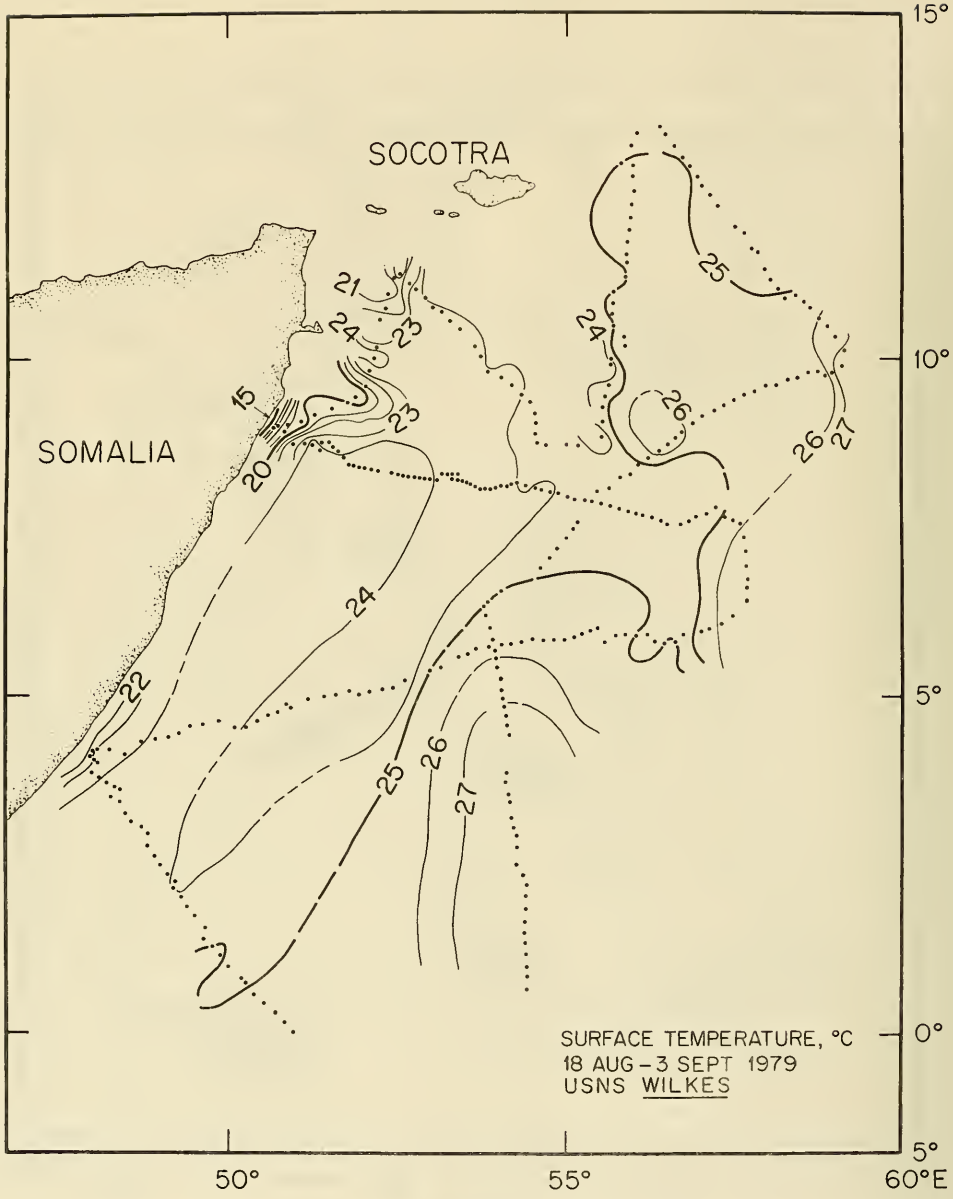
SOCOTRA
SOMALIA
15
20
21
22
23
24
25
26
27
SURFACE TEMPERATURE, °C
18 AUG – 3 SEPT 1979
USNS WILKES
15°
10°
5°
0°
5°
50°
55°
60°E

Figure 18

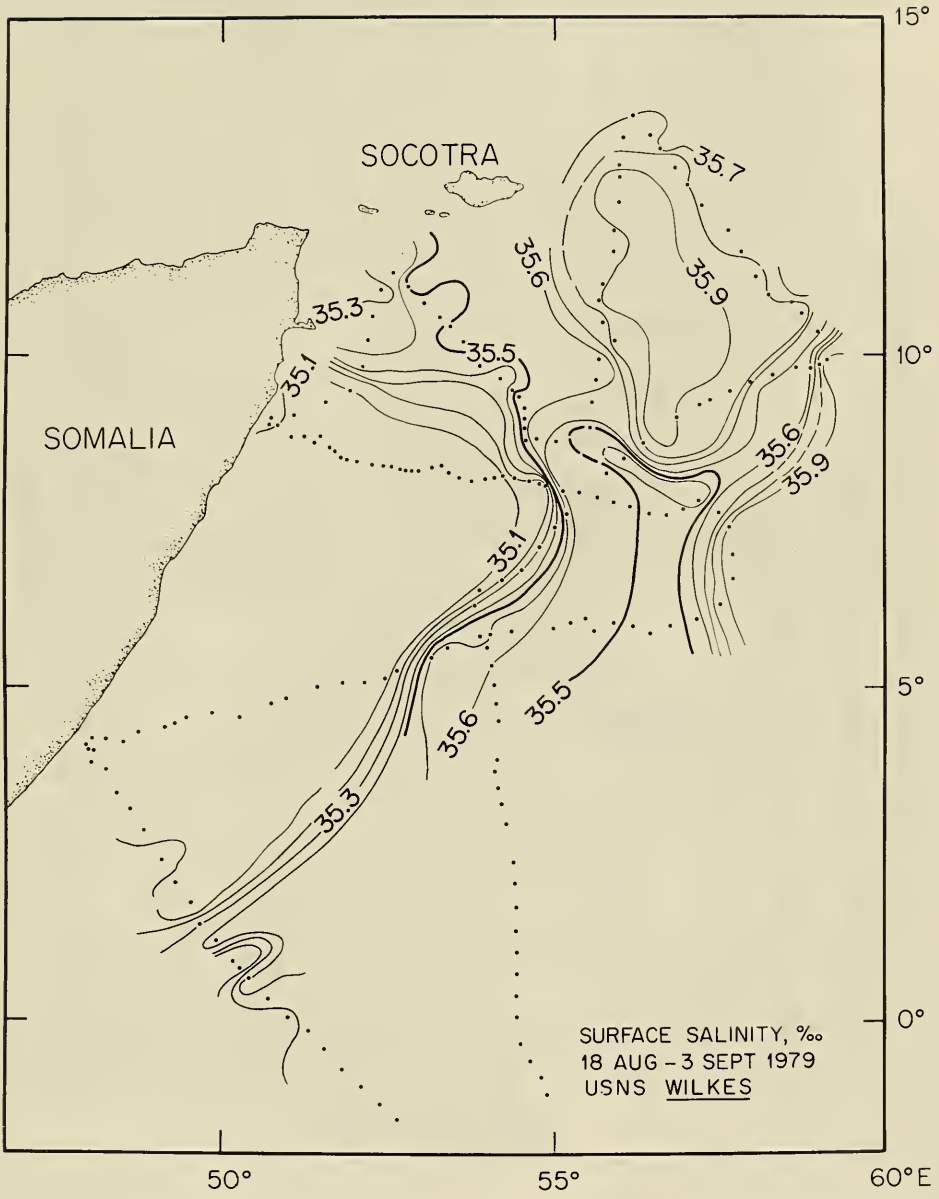
SOCOTRA
SOMALIA
35.1
35.3
35.5
35.6
35.7
35.9
SURFACE SALINITY, ‰
18 AUG - 3 SEPT 1979
USNS WILKES
15°
10°
5°
0°
50°
55°
60°E

Figure 19

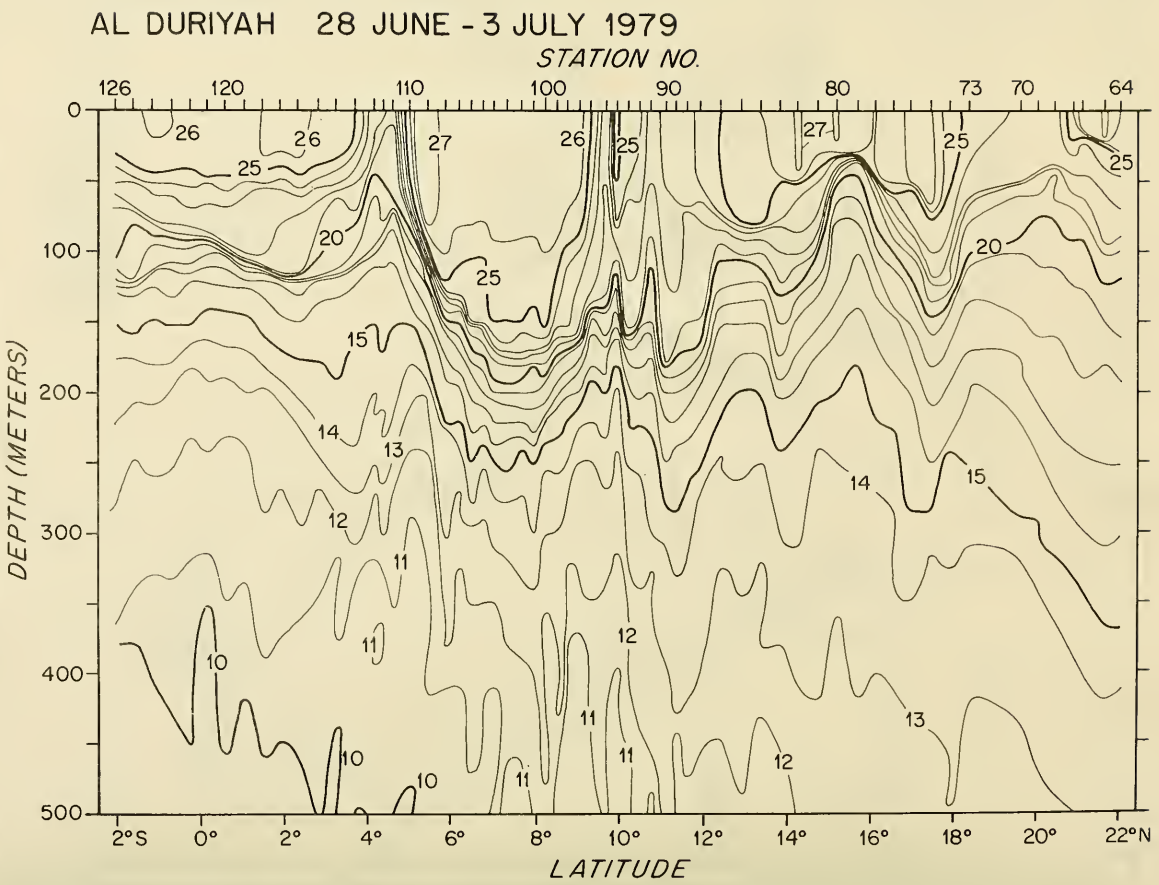

Figure 20. Temperature (°C) from XBT stations along tanker sea lane (see figure 1)

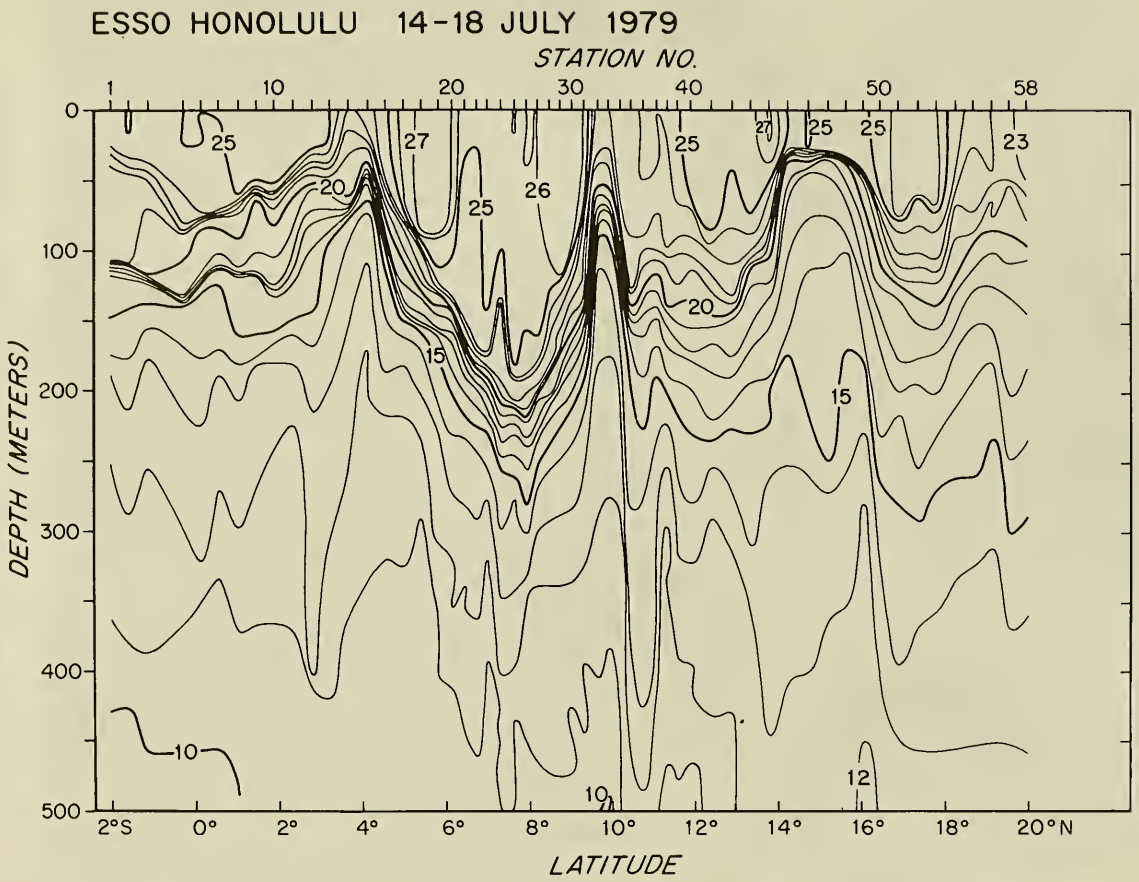

Figure 21. Temperature (°C) from XBT stations along tanker sea lane (see figure 1)

Figure 22. Satellite imagery for 2345Z, 12 July 1979, NOAA 4, Orbit 3830, VHRR

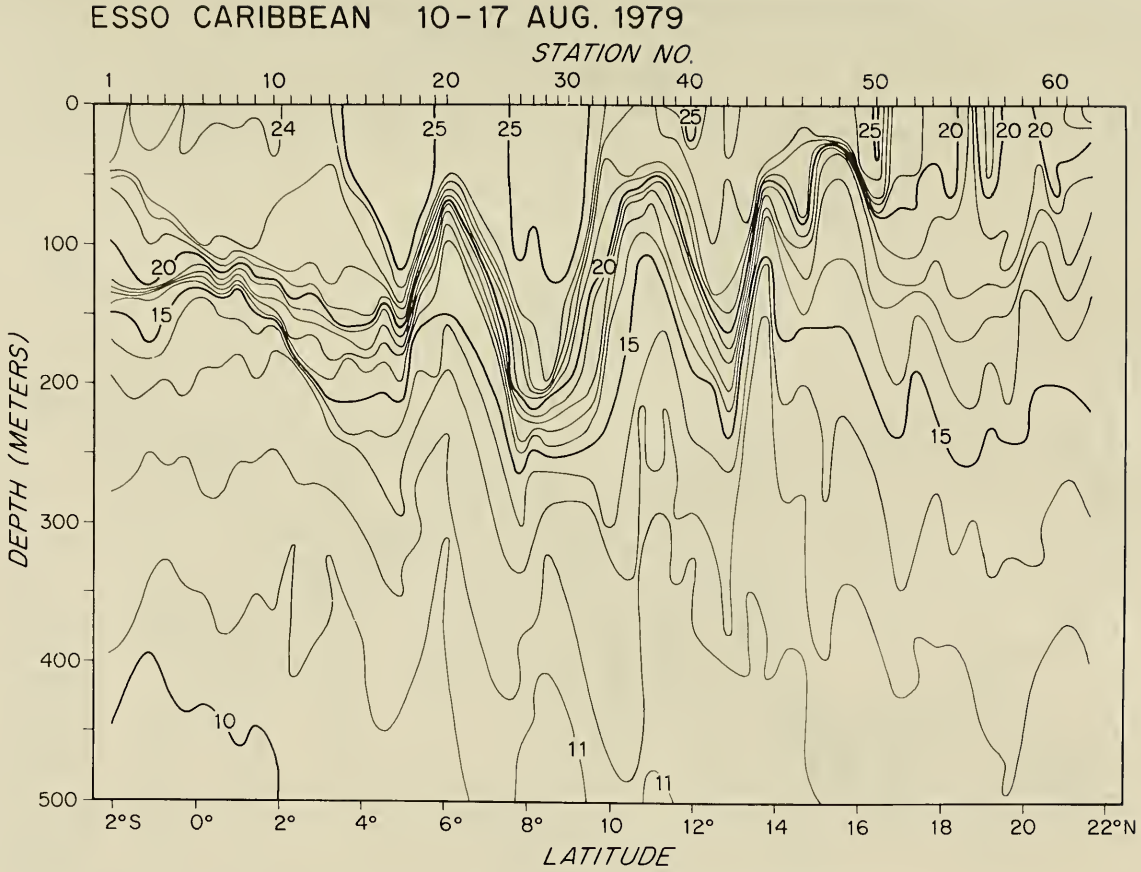

Figure 23. Temperature (°C) from XBT stations along tanker sea lane (see figure 1)

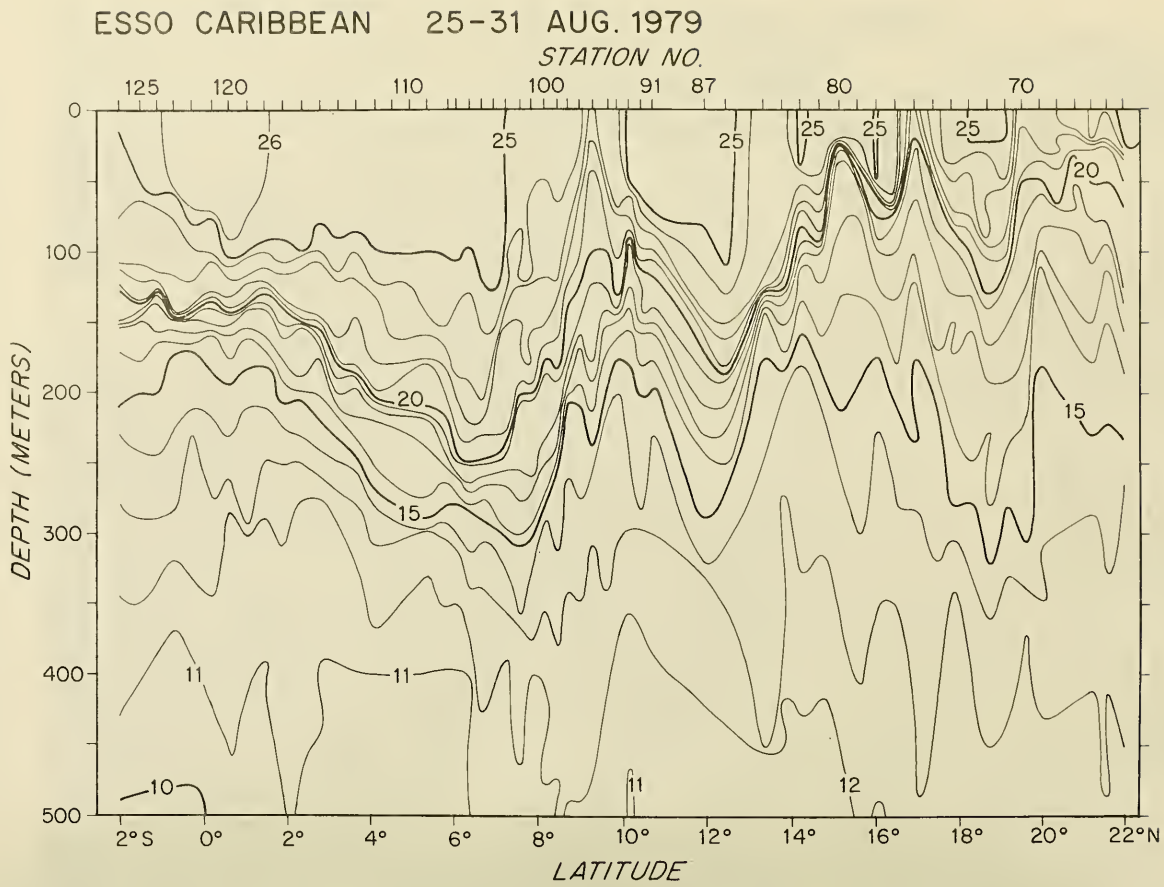

Figure 24. Temperature (°C) from XBT stations along tanker sea lane (see figure 1)

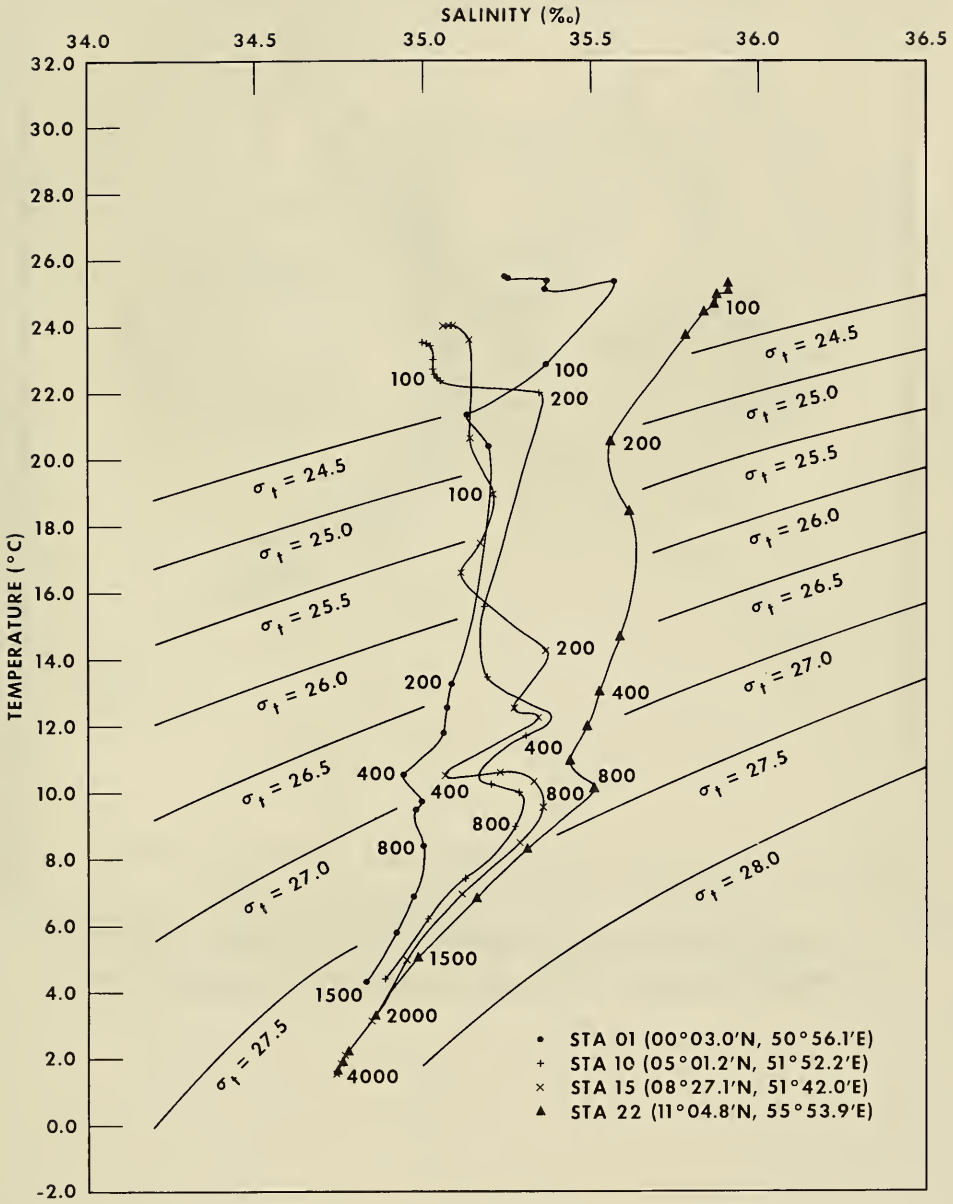

Figure 25. Temperature-Salinity (TS) Curves, Stations 1, 10, 15, 22

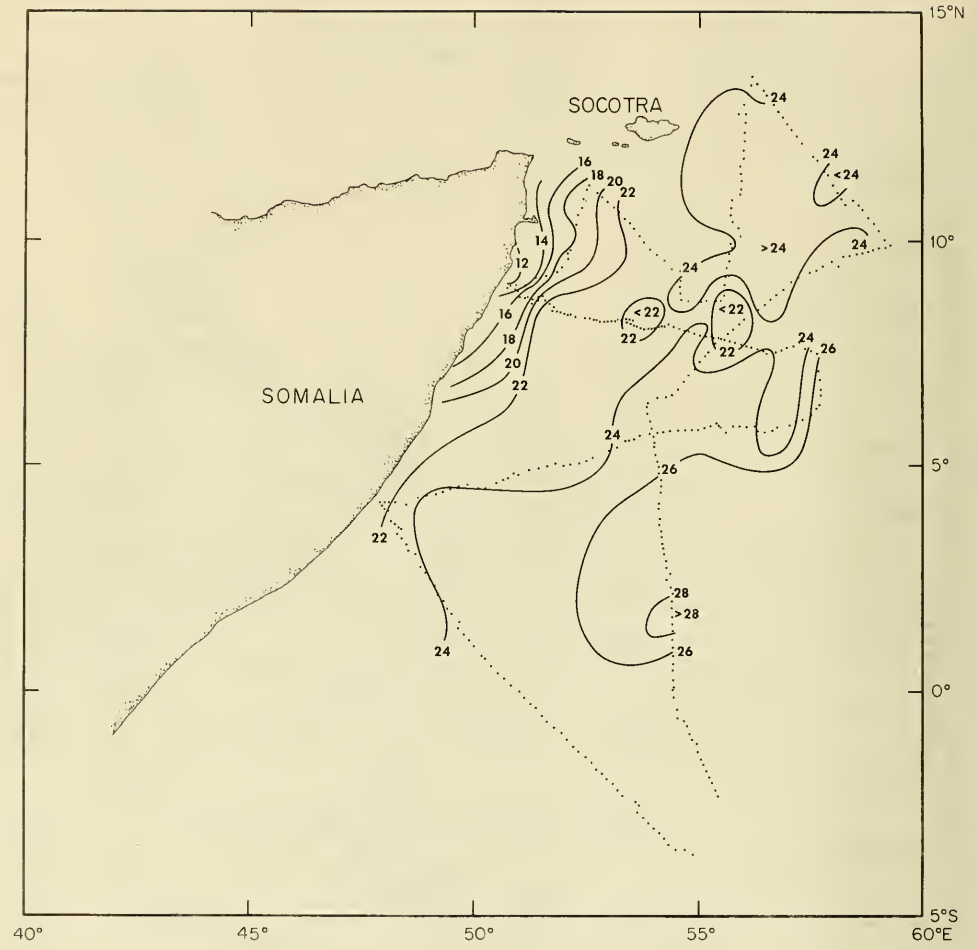

Figure 26. Temperature (°C) at 50m depth, USNS WILKES, 18 August - 3 September 1979

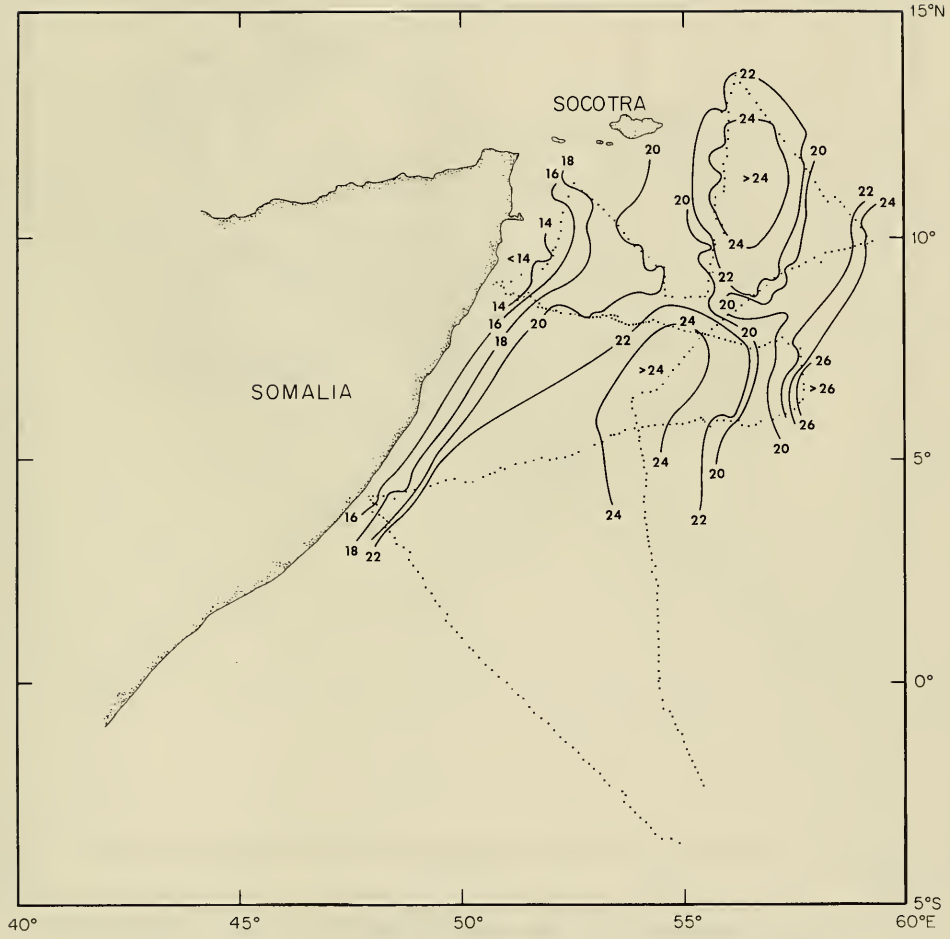

Figure 27. Temperature (°C) at 100m depth, USNS WILKES, 18 August - 3 September 1979

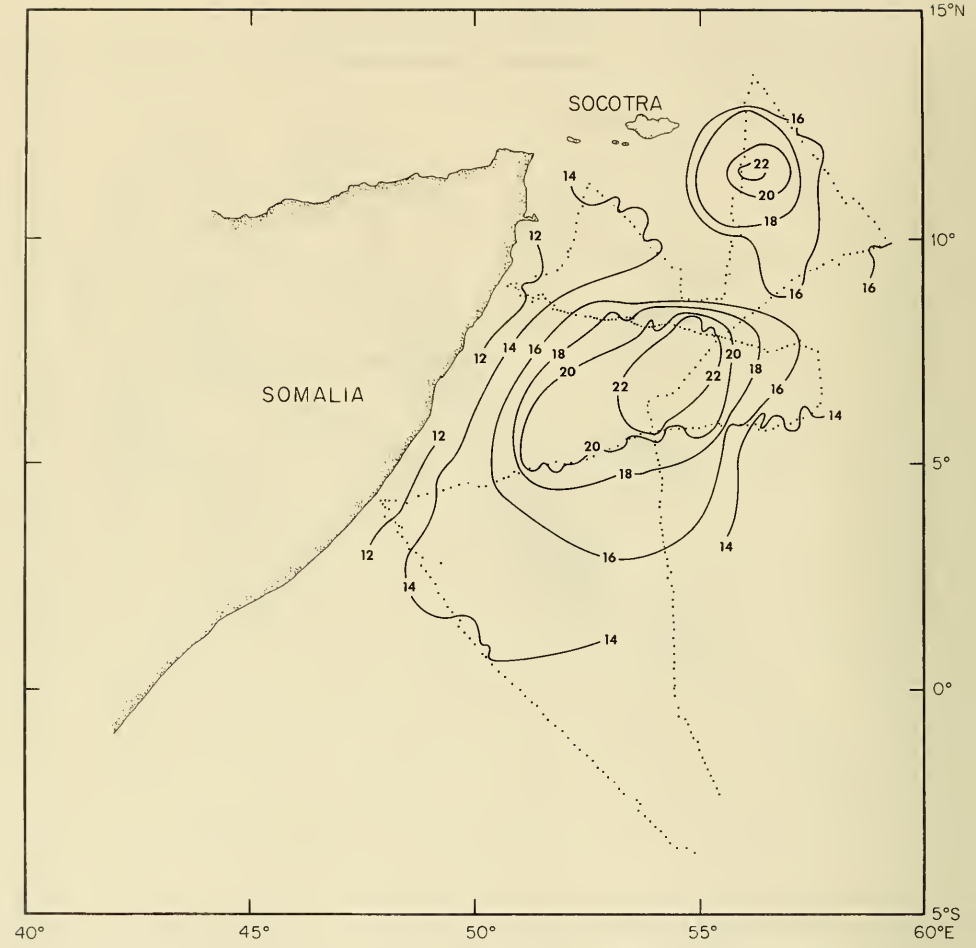

Figure 28. Temperature (°C) at 200m depth, USNS WILKES, 18 August - 3 September 1979

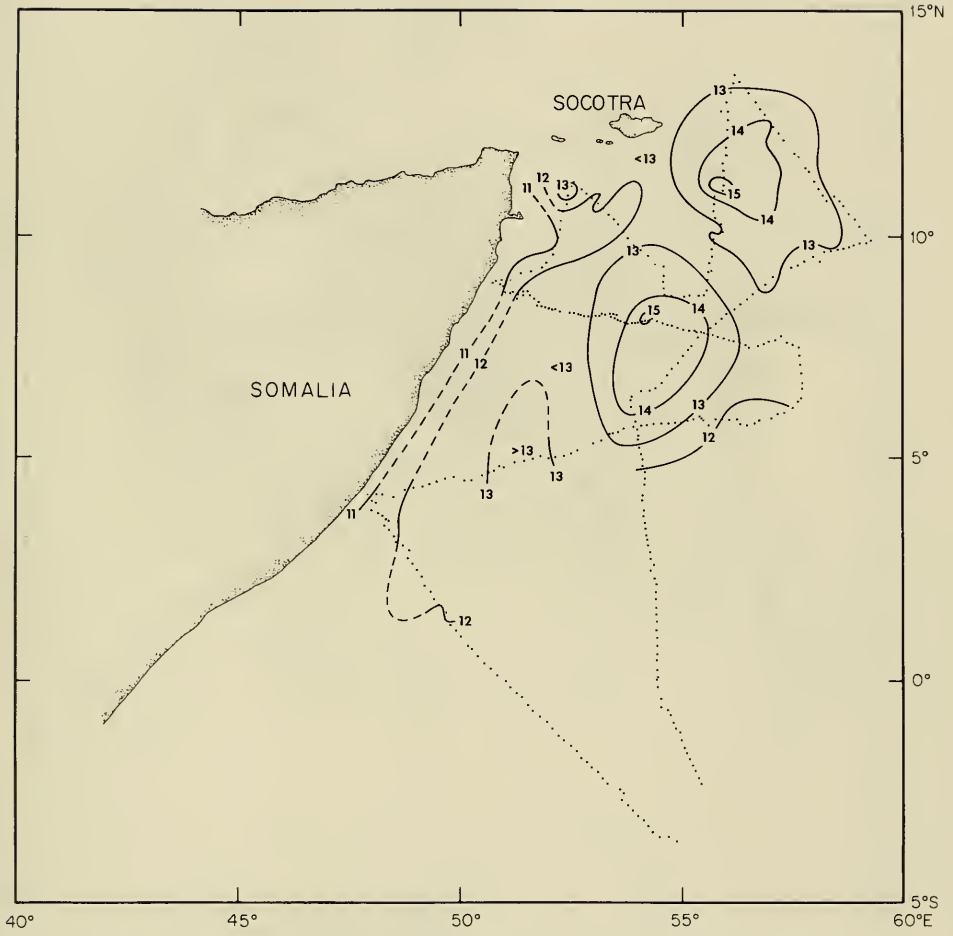

Figure 29. Temperature (°C) at 300m depth, USNS WILKES, 18 August - 3 September 1979

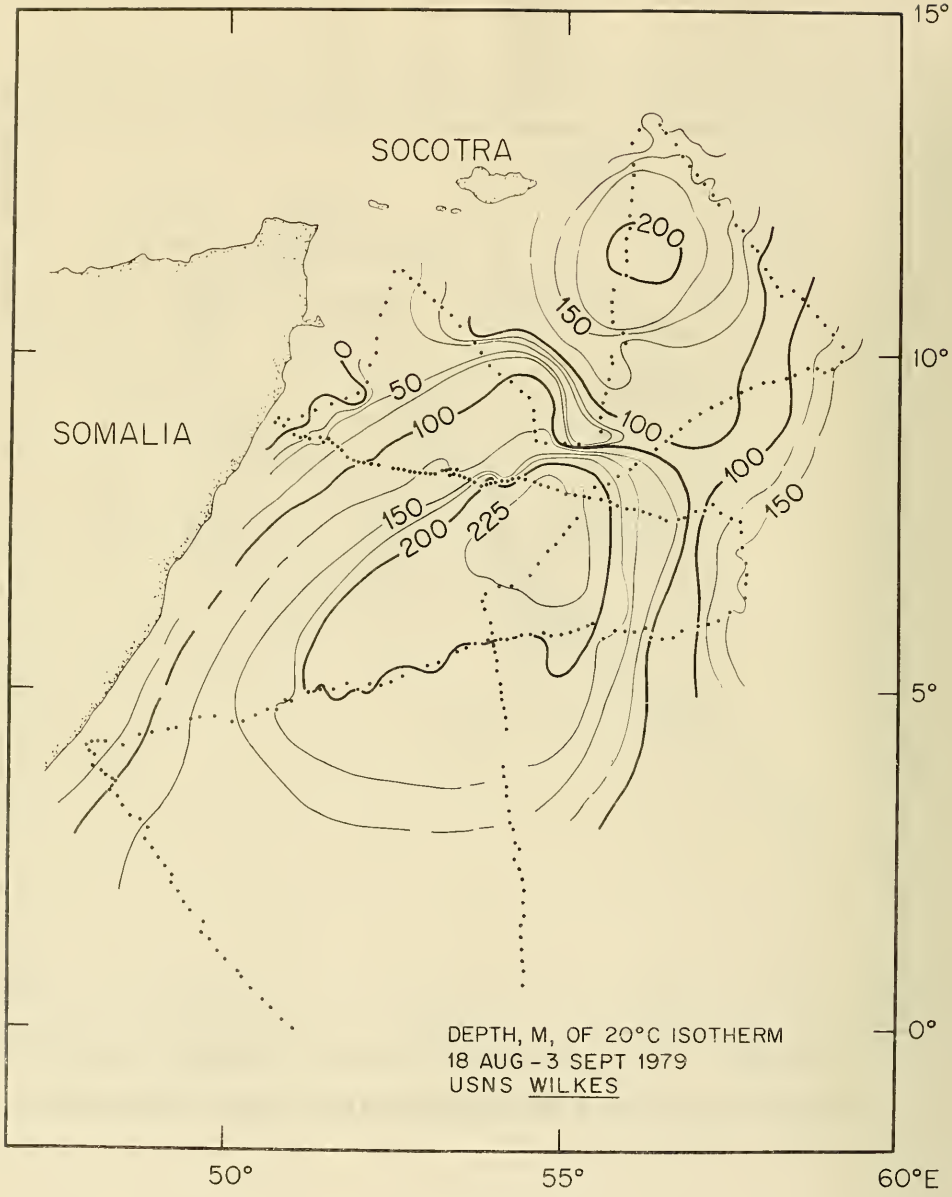
SOCOTRA
SOMALIA
0
50
100
150
200
225
100
100
150
200
150
DEPTH, M, OF 20°C ISOTHERM
18 AUG - 3 SEPT 1979
USNS WILKES
15°
10°
5°
0°
50°
55°
60°E

Figure 30

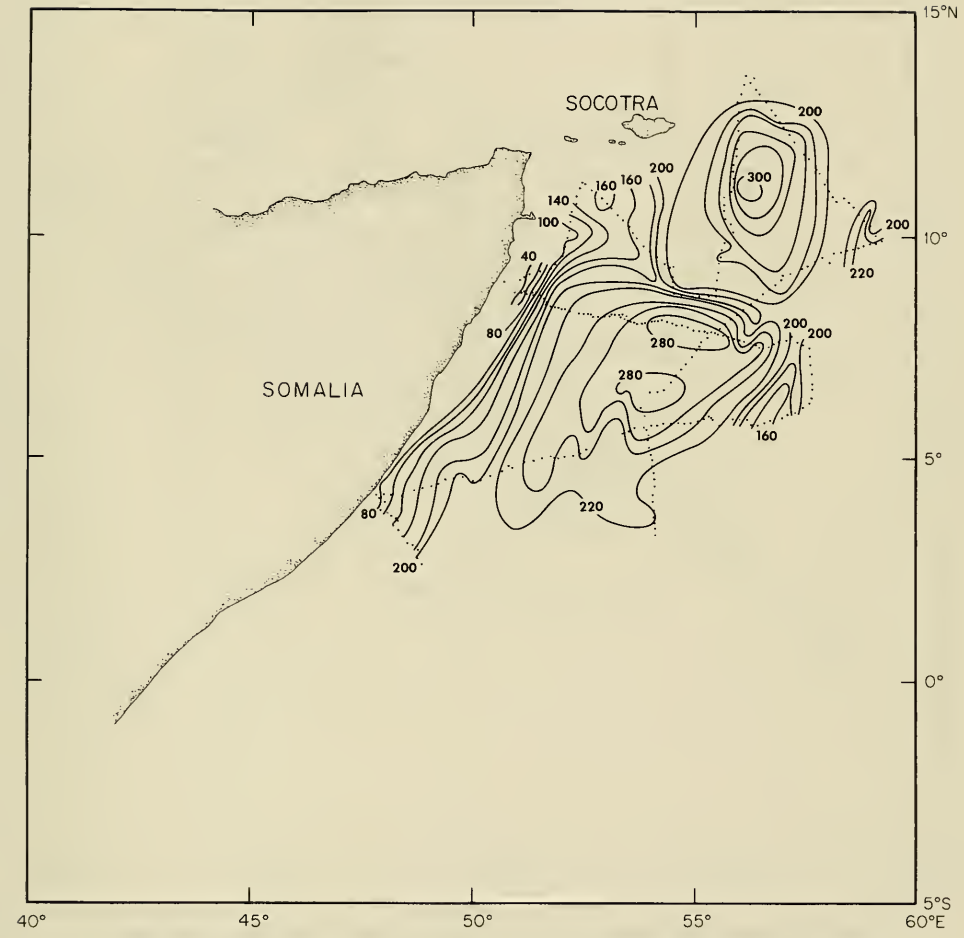

Figure 31. Depth (m) of 15°C isotherm, USNS WILKES, 18 August - 3 September 1979

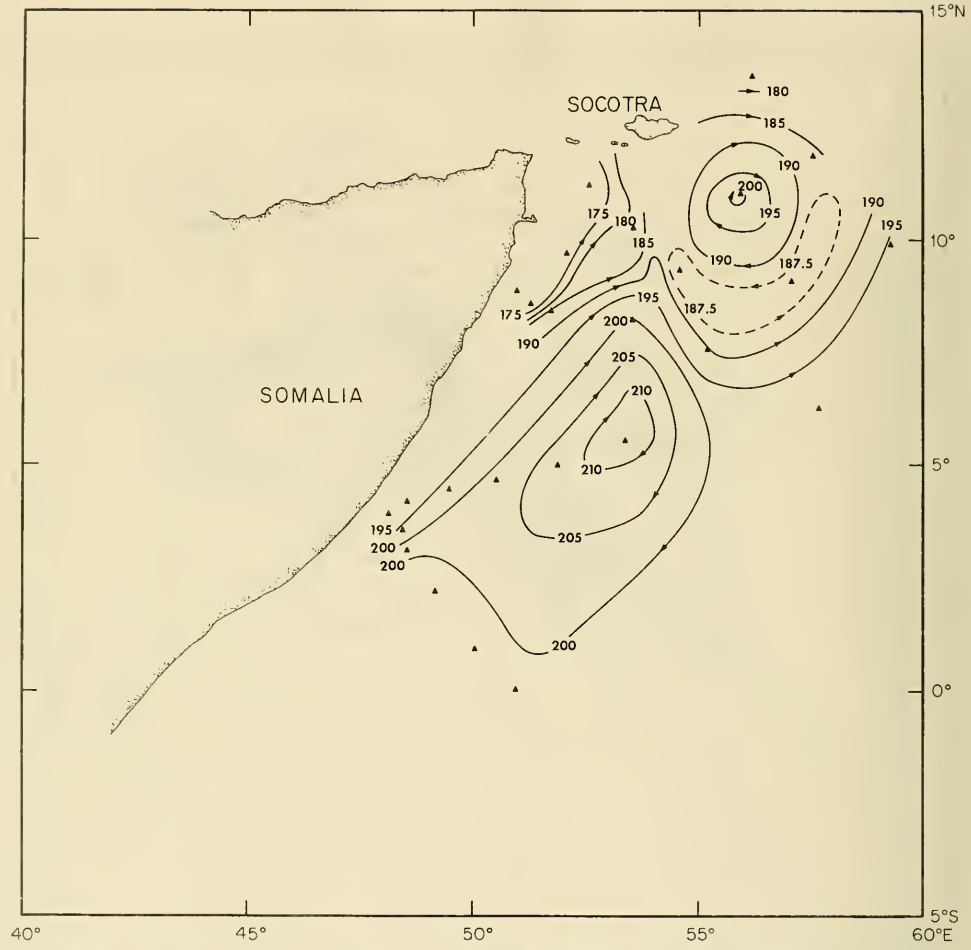

Figure 32. Dynamic topography (dyn cm) of surface relative to 1500 dbar, USNS WILKES, 18 August - 3 September 1979

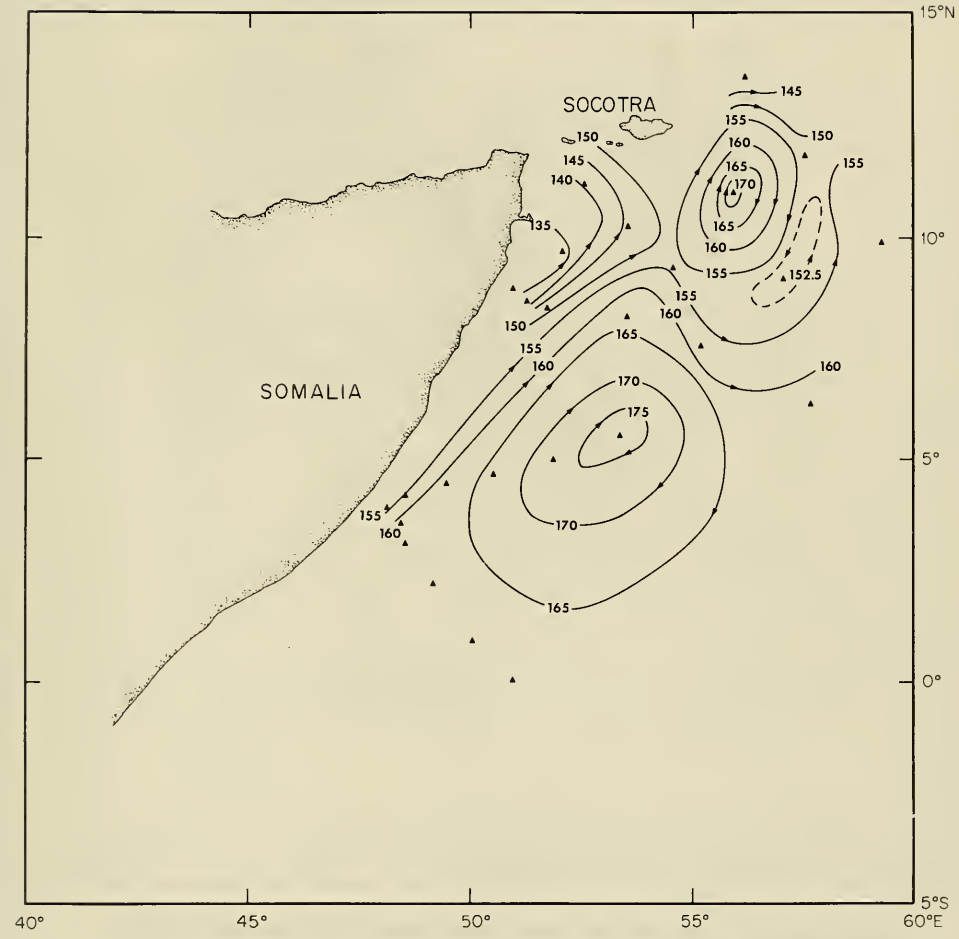

Figure 33. Dynamic Topography (dyn cm) of surface relative to 1000 dbar, USNS WILKES, 18 August - 3 September 1979

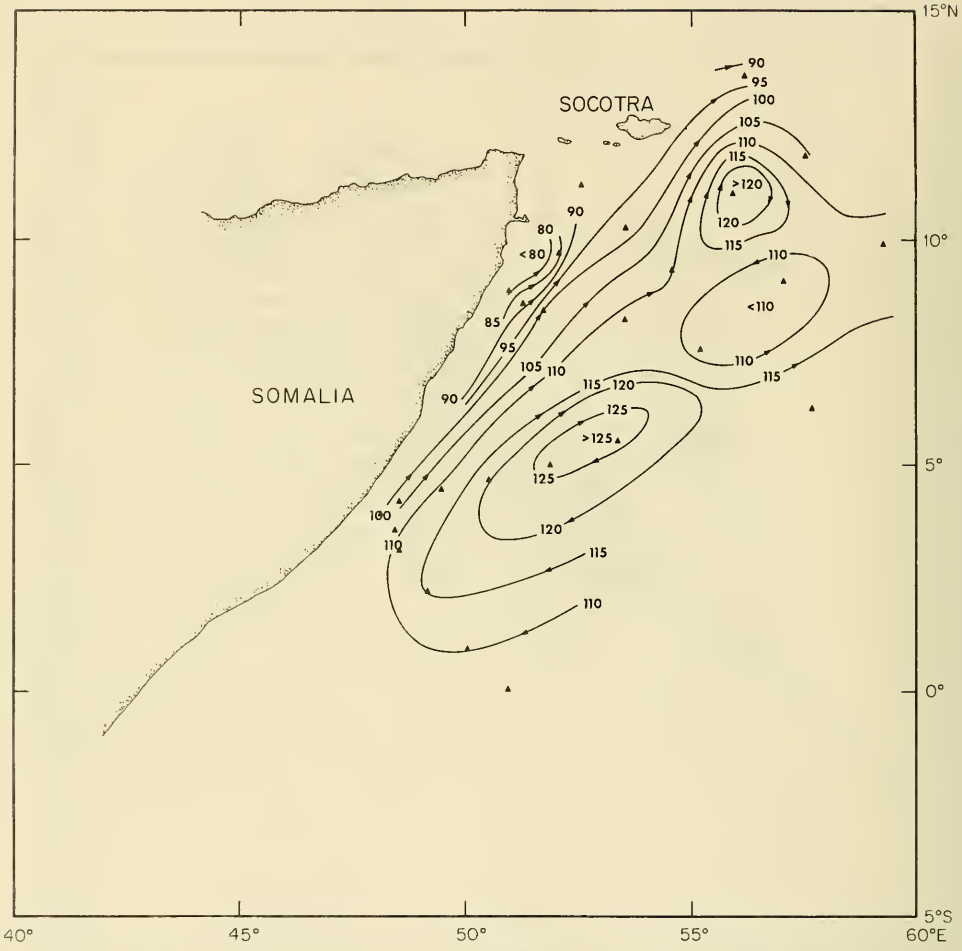

Figure 34. Dynamic Topography (dyn cm) of surface relative to 500 dbar, USNS WILKES, 18 August - 3 September 1979

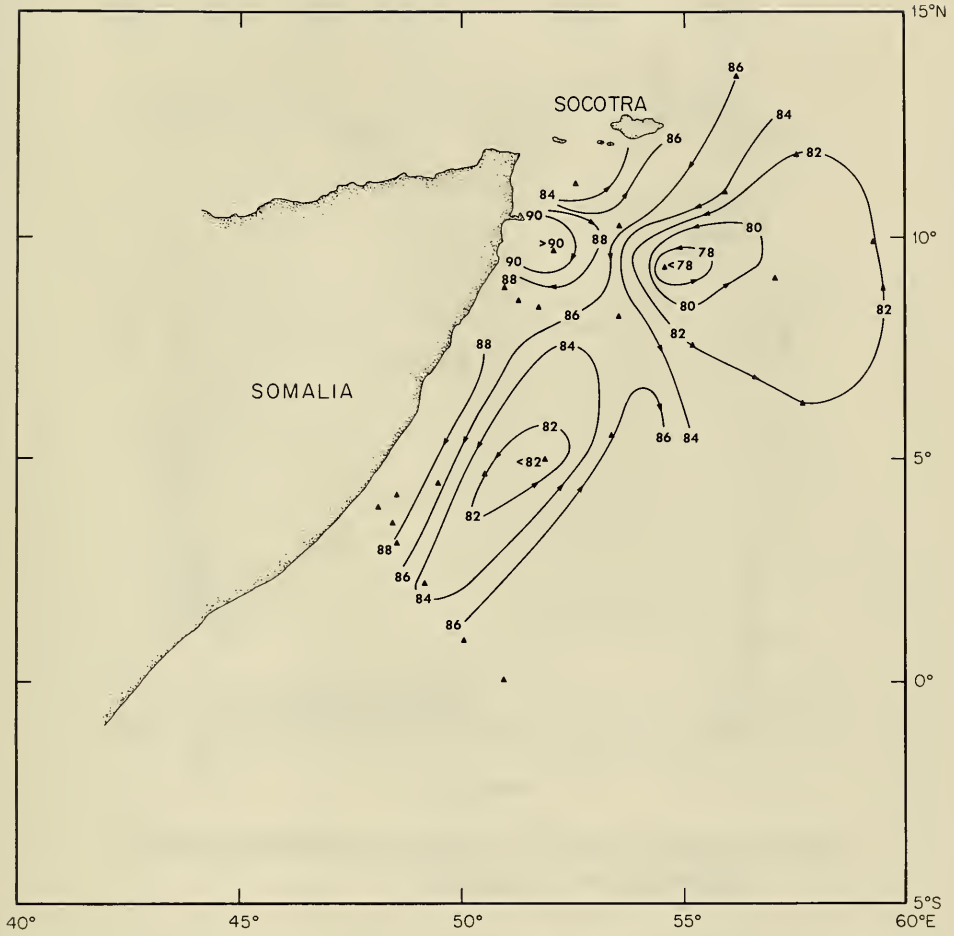

Figure 35. Dynamic Topography (dyn cm) of 500 dbar relative to 1500 dbar, USNS WILKES, 18 August - 3 September 1979

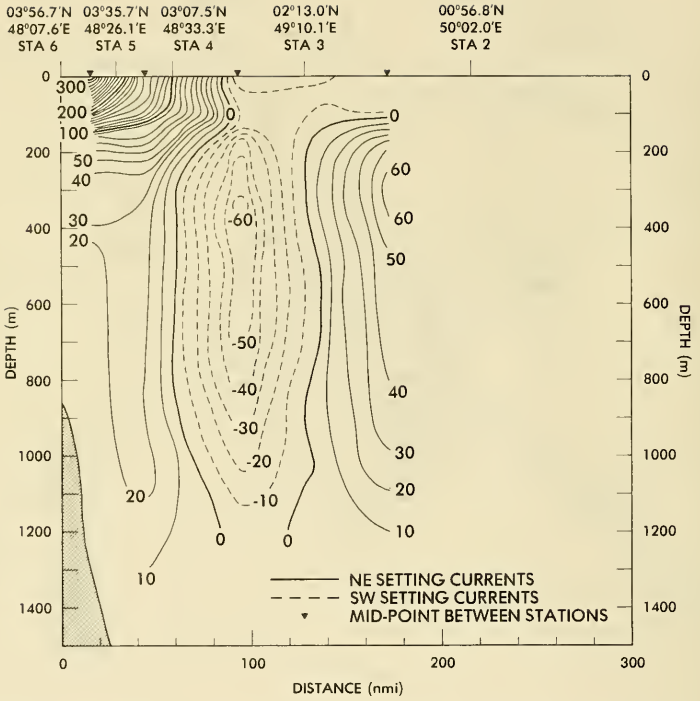

Figure 36. Geostrophic currents (cm sec^{-1}) relative to 1500 dbar across Section 1, USNS WILKES, 16 - 19 August 1979

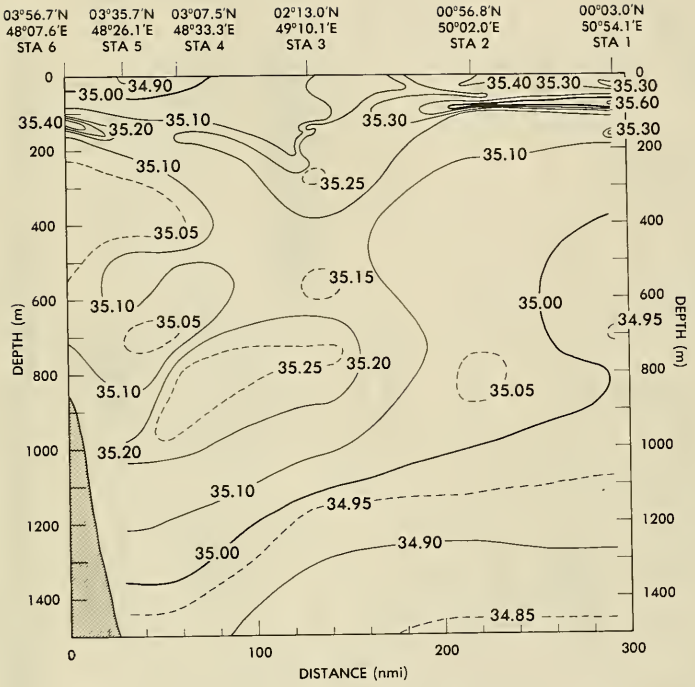

Figure 37. Salinities (‰) along Section 1, USNS WILKES, 16 - 19 August 1979

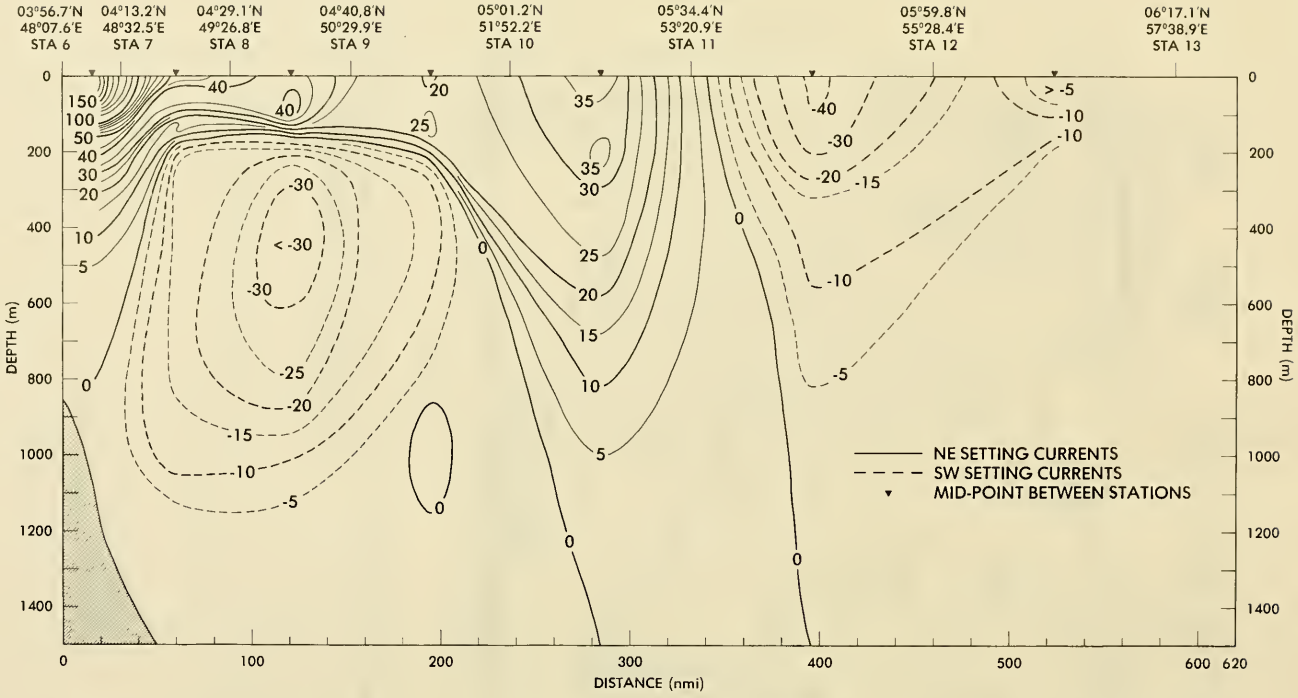

Figure 38. Geostrophic currents (cm sec^{-1}) relative to 1500 dbar across Section 2, USNS WILKES, 19 - 22 August 1979

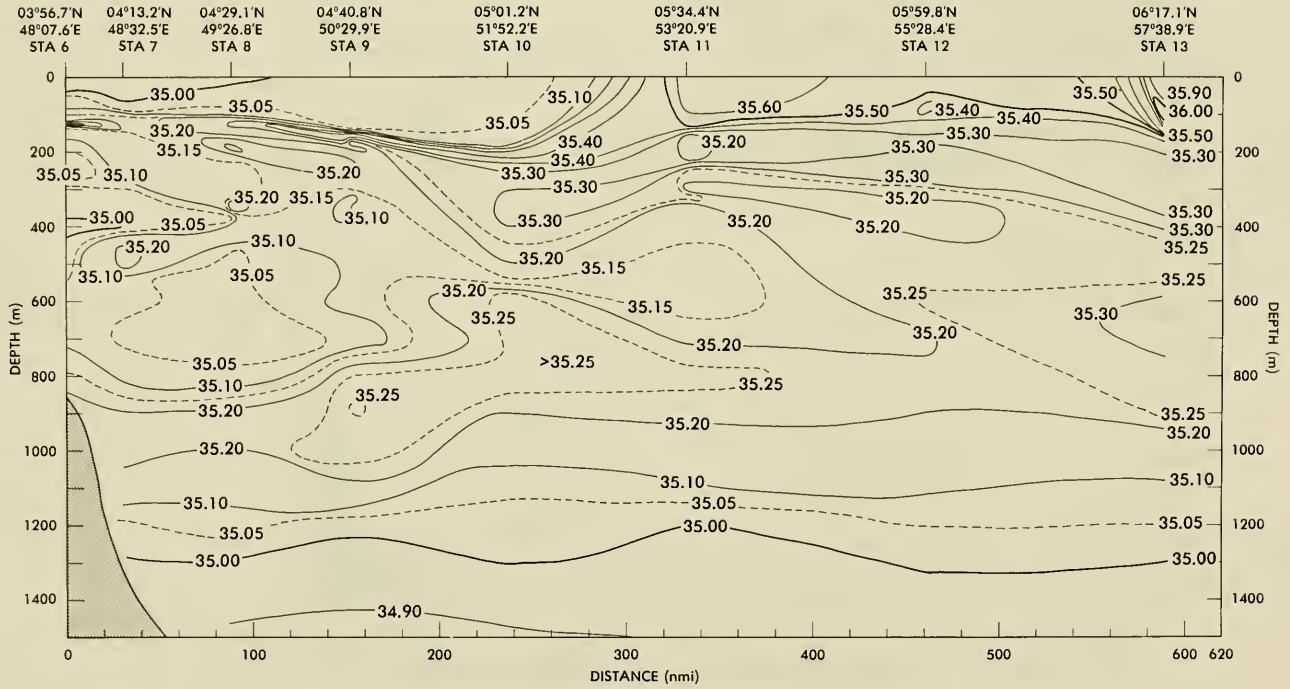

Figure 39. Salinities (‰) along Section 2, USNS WILKES, 19 - 22 August 1979

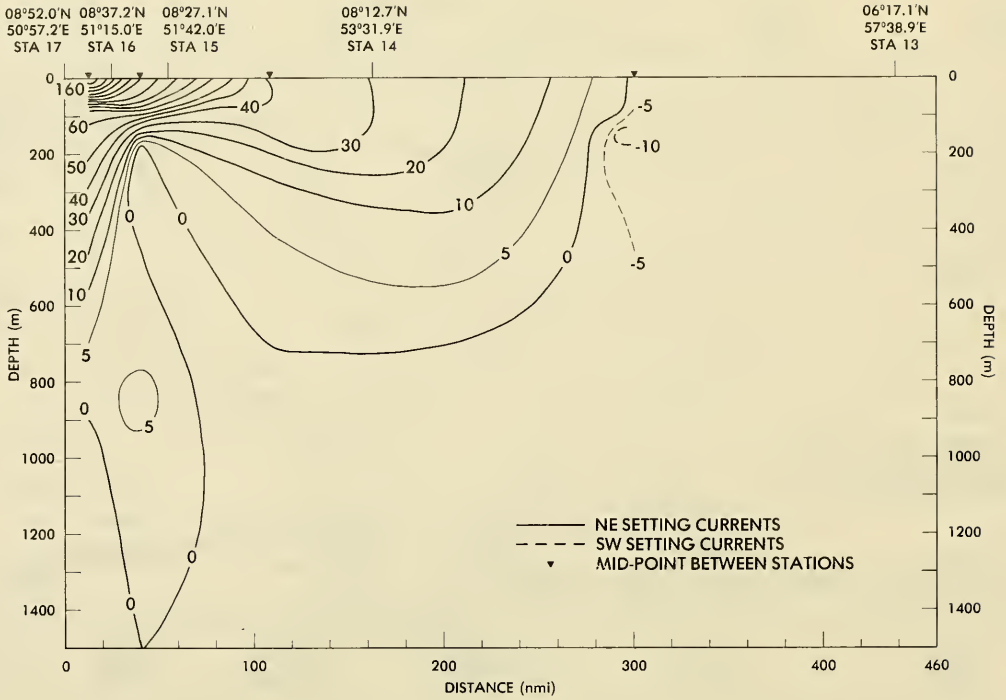

Figure 40. Geostrophic currents (cm sec^{-1}) relative to 1500 dbar across Section 4, USNS WILKES, 22 - 26 August 1979

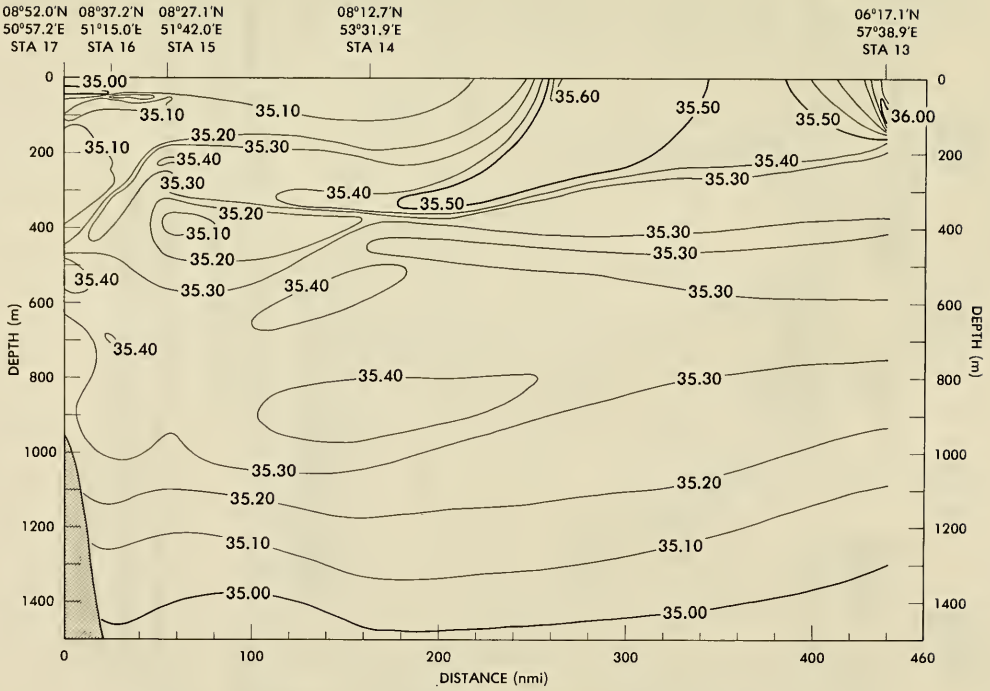

Figure 41. Salinities (‰) along Section 4, USNS WILKES, 22 - 26 August 1979

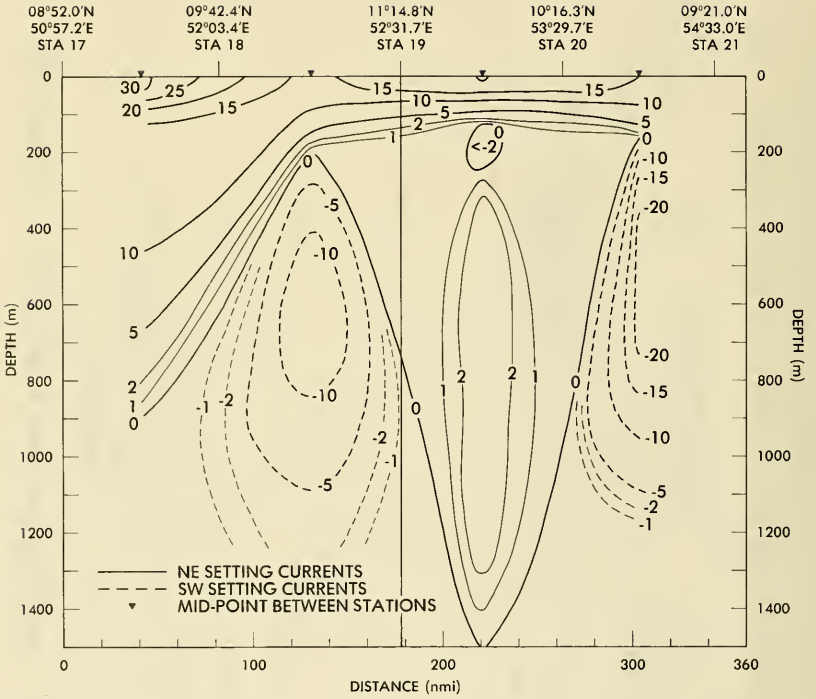

Figure 42. Geostrophic currents (cm sec^{-1}) relative to 1500 dbar across Sections 5 and 6. Section 5 is left of solid line at Station 19. USNS WILKES, 26 - 28 August 1979

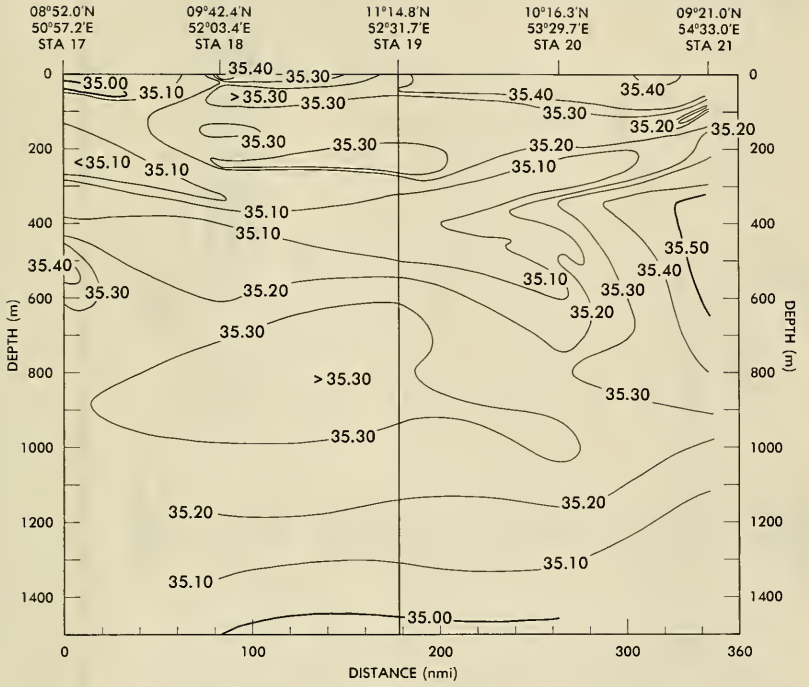

Figure 43. Salinities (‰) along Section 5 and 6. Section 5 is left of solid line at Station 19. USNS WILKES, 26 - 28 August 1979

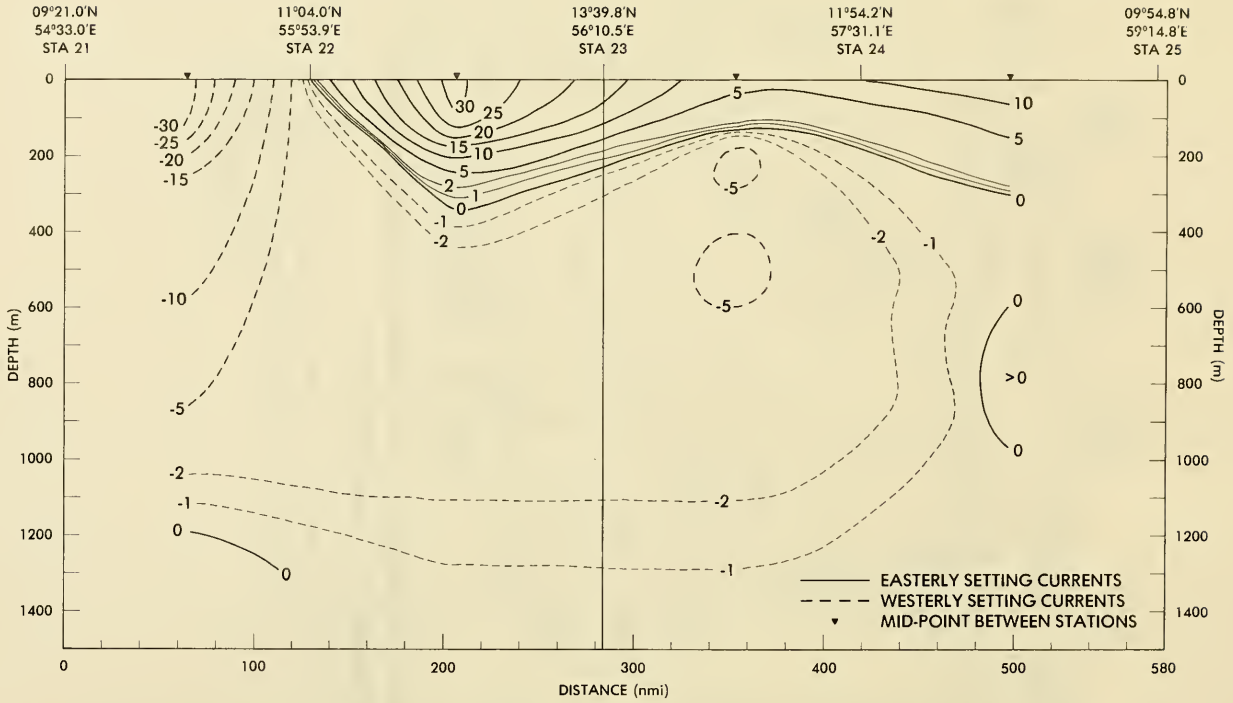

Figure 44. Geostrophic currents (cm sec^{-1}) relative to 1500 dbar across Sections 7 and 8. Section 7 is left of solid line at Station 23. USNS WILKES, 28 - 31 August 1979

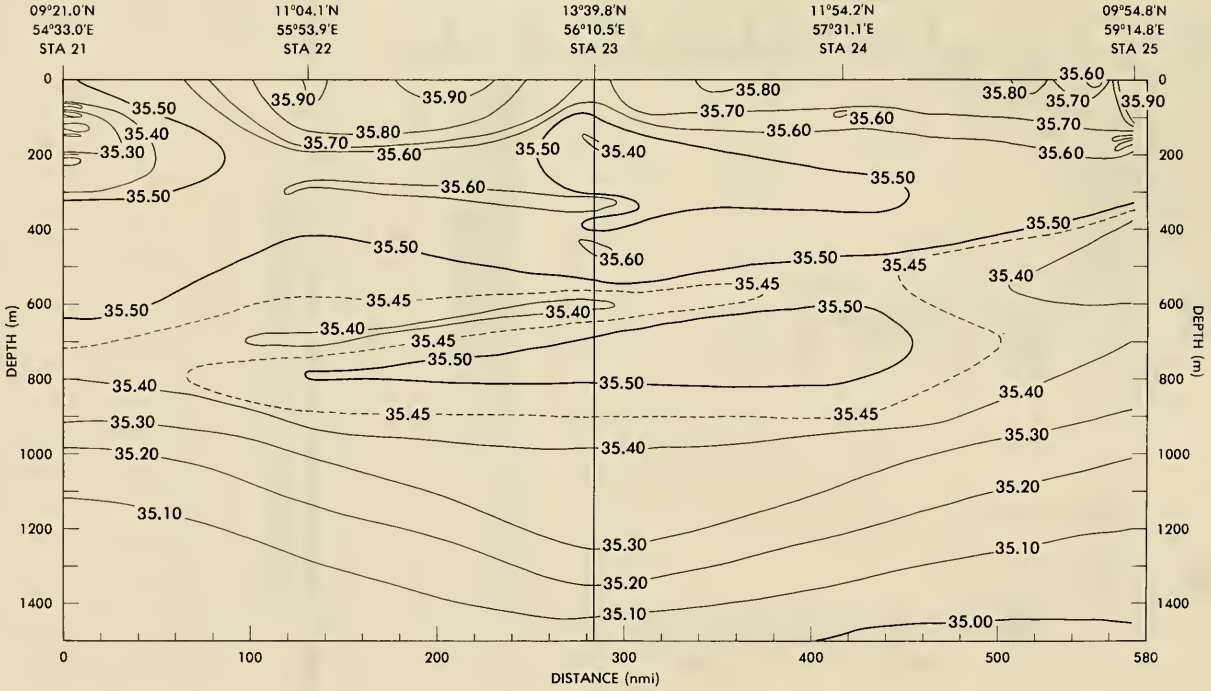

Figure 45. Salinities (‰) along Sections 7 and 8. Section 7 is left of solid line at Station 23. USNS WILKES, 28 - 31 August 1979

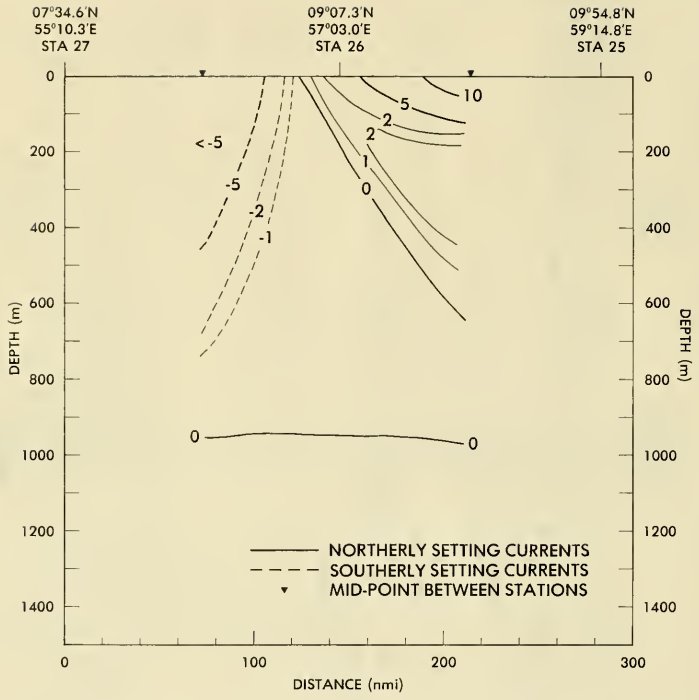

Figure 46. Geostrophic currents (cm sec^{-1}) relative to 1500 dbar across Section 9, USNS WILKES, 31 August - 2 September 1979

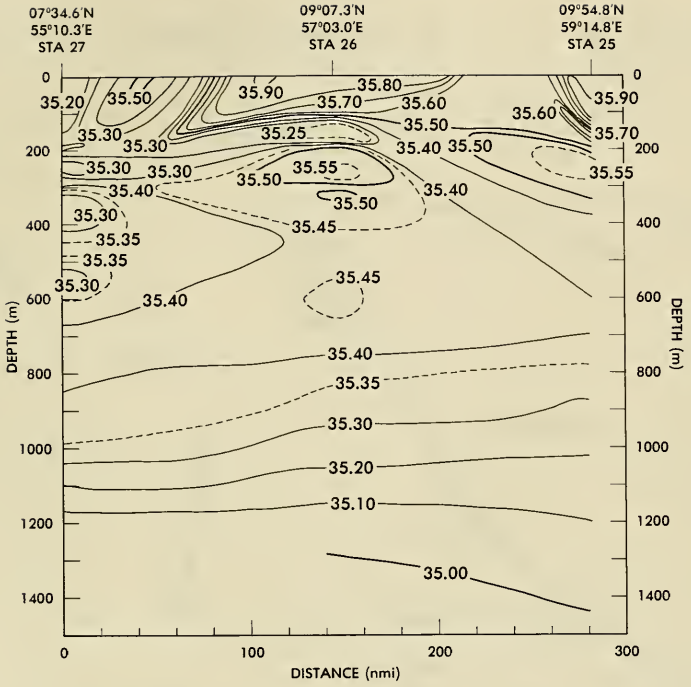

Figure 47. Salinities (‰) along Section 9, USNS WILKES, 31 August - 2 September 1979

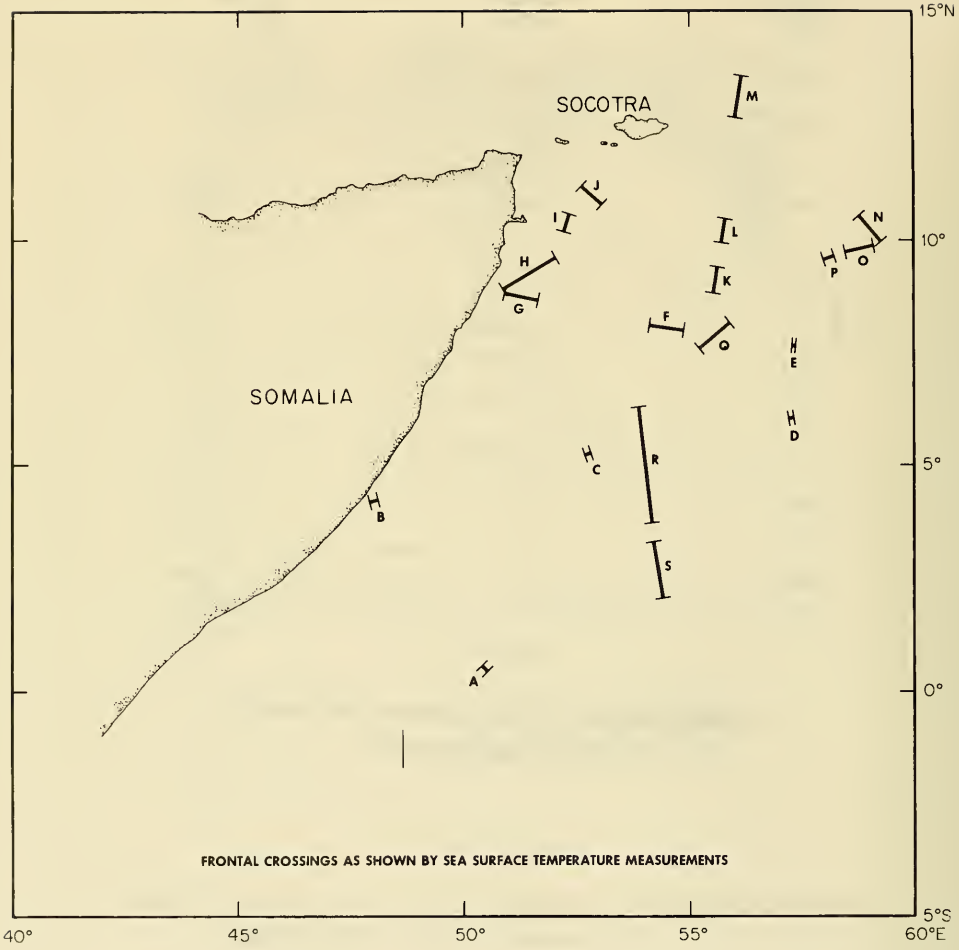

Figure 48. Locations of sea surface thermal discontinuities measured by hull-mounted thermometer, USNS WILKES, 18 August - 3 September 1979

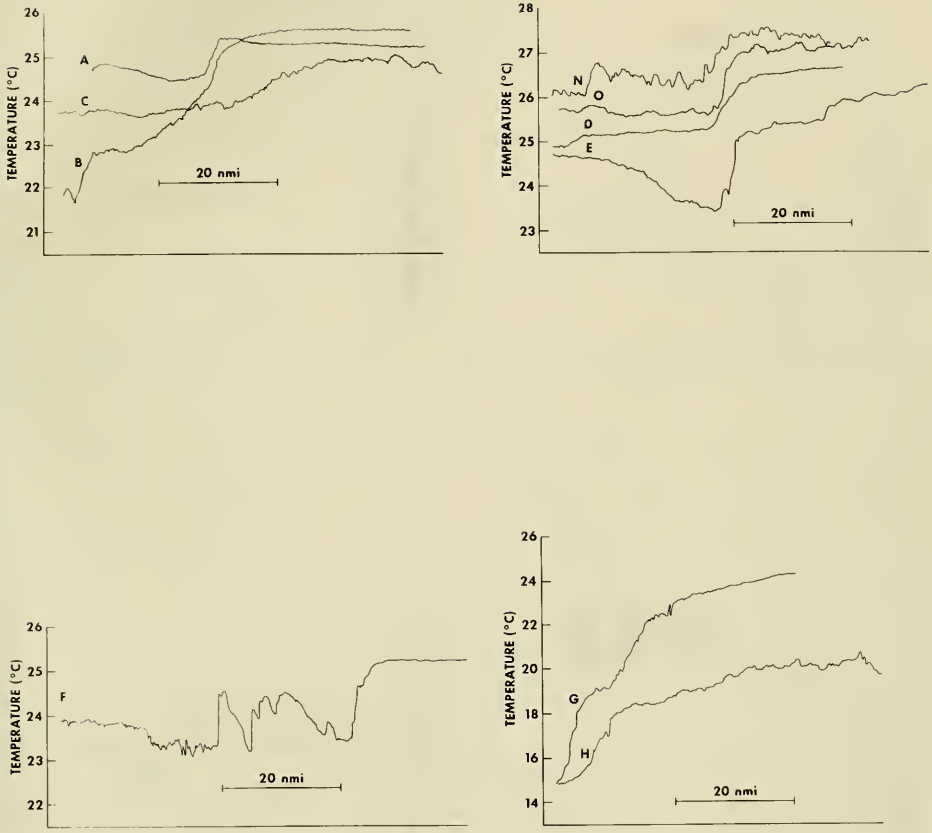

Figure 48a. Continuous sea surface analog temperature (°C) traces made across thermal discontinuities between 18 and 31 August 1979 (see figure 48). Values to the left of thermal discontinuities give temperatures within regions of cool, upwelled water

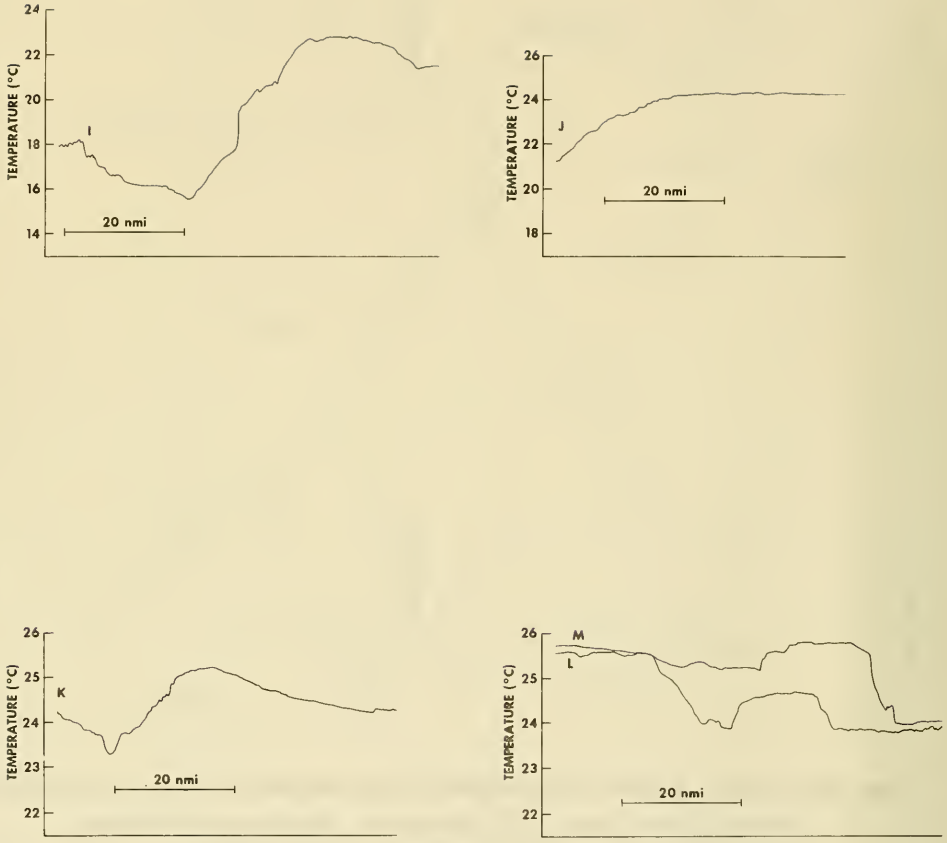

Figure 48b. Continuous sea surface analog temperature (°C) traces made across thermal discontinuities between 26 and 30 August 1979 (see figure 48). Values to the left in traces I, J, and K give temperatures in cool, upwelled water of coastal origin. Values to the left in traces L and M give temperatures in the interior of the Socotra Eddy

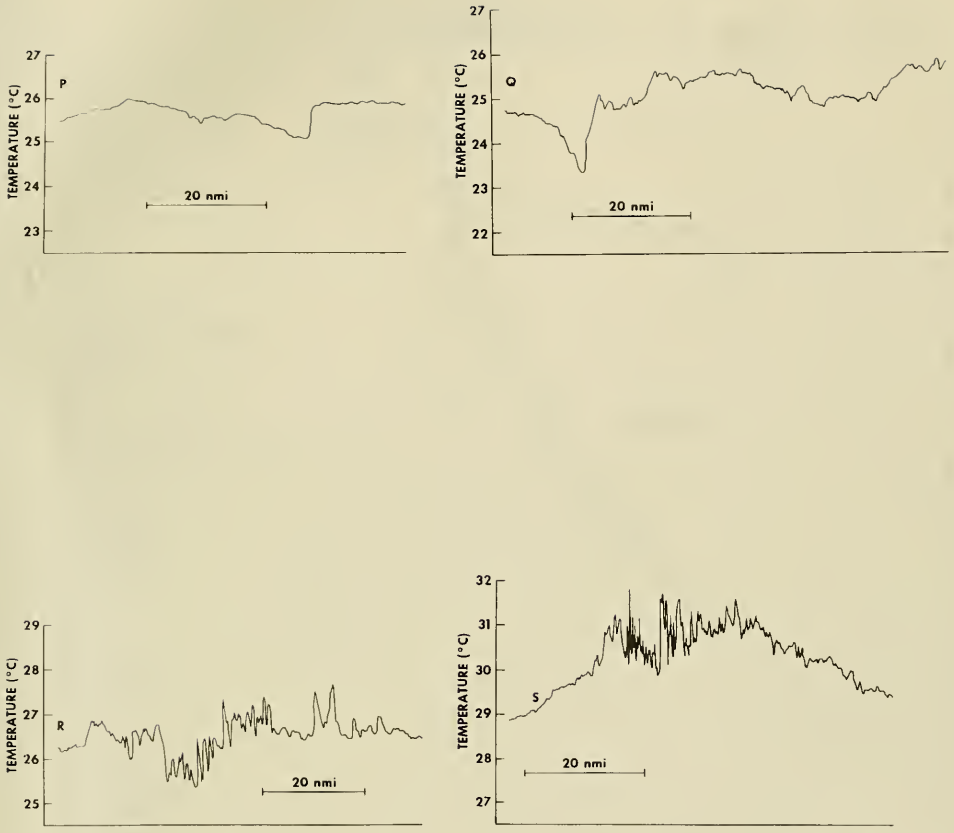

Figure 48c. Continuous sea surface analog temperature (°C) traces made across thermal discontinuities between 31 August and 3 September 1979 (see figure 48). Values to the right in trace P give temperatures in southeastern corner of Socotra Eddy. Values to the right in trace Q give temperatures in northern edge of great whirl. Traces R and S are oriented north-south with values to the left giving temperatures at northern ends of traces

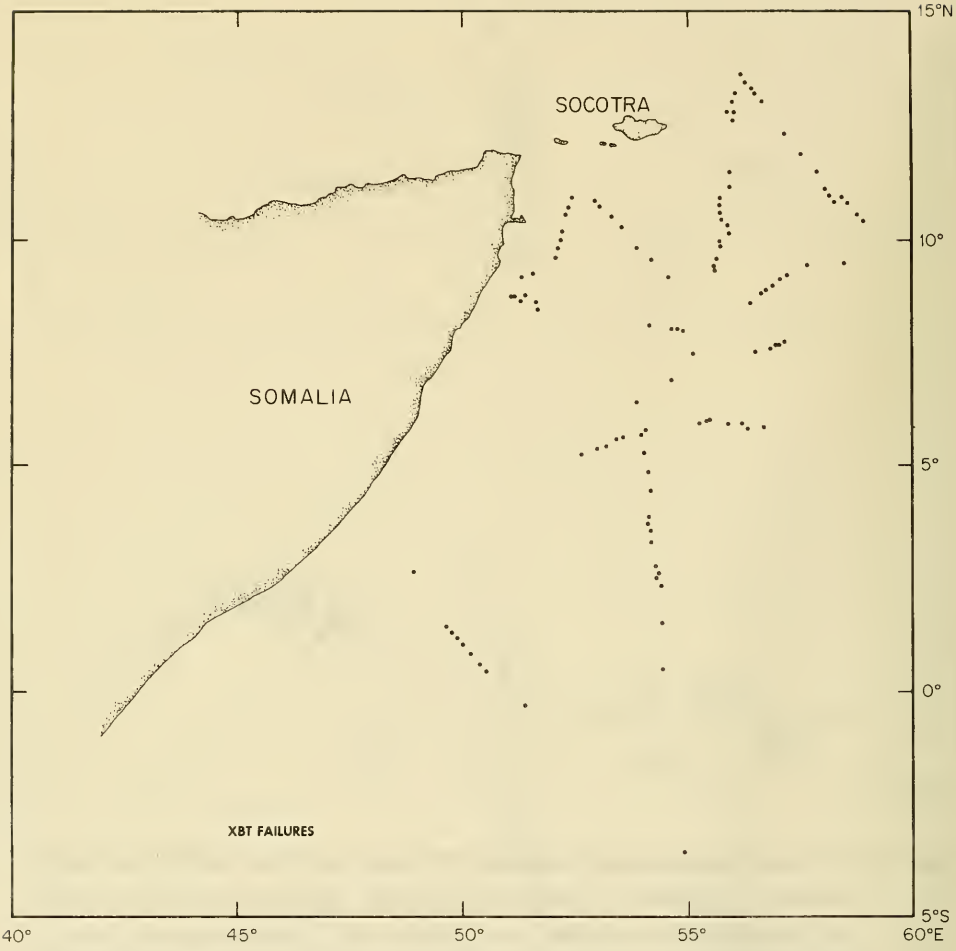

Figure 49. Location of XBT failures, USNS WILKES, 18 August - 3 September 1979

DISTRIBUTION LIST

CNO (OP-095, -0952) 1 each	2
COMNAVOCEANCOM	1
UNSECDEF (R&E)	1
NAVWARCOL	1
ASN (R&D)	1
CNR (Code 480)	1
NISC	1
NORDA	1
NRL	1
USNA	1
NUSC-Newport	2
NUSC-New London	2
NAVPGSCOL	2
NOSC	2
ONR-Pasadena	1
ONR-Boston	1
SWOSCOLCOM	1
CIA	1
NASA/GSFC	1
NOAA/NOS	1
OSC/NU	1
DM/ UCLA	1
DGS/UC	1
LDGO	1
DO/FSU	1
DO/MC/UH	1
DEPS/JHU	1
DM/MIT	1
RSMAS/UM	1
DAOS/UM	1
UIO/CCCUNY	1
DMO/PINY	1
DS/SUNYMC	1
IO/ODU	2
SO/OSU	1
CEMS/PSU	1
GSO/URI	1
DO/TAMU	1
DO/UW	1
SIO	1
PMEL/UW	1
AOML/UM	1
DM/UW	1
JPL	1
EXXON	1
WHOI	2
NEUMANN	1
CSIRO-Australia	1
IOS-England	1
MHN-France	1
NIO-India	1
EAMFRO-Kenya	1

DISTRIBUTION LIST (CON'D)

USCG/RDC-New London	1
GI/POD/UB-Norway	2
MFMT-Somalia	1
CSIRO-South Africa	1
UCT-South Africa	1
GARPAO/WMO-Switzerland	1
EAMFRO-Tanzania	1
DTIC	12

CIRCULATION AND OCEANOGRAPHIC PROPERTIES IN THE SOMALI BASIN AS OBSERVED DURING THE 1979 SOUTHWEST MONSOON

WILLIAM H. BEATTY III
JOHN G. BRUCE
ROBERT C. GUTHRIE

JUNE 1981